Physics of Fluids

RESEARCH ARTICLE | NOVEMBER 21 2023

Small-amplitude waves in a floating poroelastic plate forcing by vertical pitching plate

Q. Y. Wu (吴其远) ; T. I. Khabakhpasheva ; B. Y. Ni (倪宝玉) ; A. A. Korobkin

Physics of Fluids 35, 117127 (2023)
https://doi.org/10.1063/5.0175412

Physics of Fluids ARTICLE pubs.aip.org/aip/pof

Small-amplitude waves in a floating poroelastic plate forcing by vertical pitching plate

Cite as: Phys. Fluids **35**, 117127 (2023); doi: 10.1063/5.0175412
Submitted: 6 September 2023 · Accepted: 28 October 2023 ·
Published Online: 21 November 2023

Q. Y. Wu (吴其远),[1] T. I. Khabakhpasheva,[2,3,a)] B. Y. Ni (倪宝玉),[1] and A. A. Korobkin[2]

AFFILIATIONS

[1]College of Shipbuilding Engineering, Harbin Engineering University, Harbin 150001, China
[2]School of Mathematics, University of East Anglia, Norwich NR4 7TJ, United Kingdom
[3]Lavrentyev Institute of Hydrodynamics, Novosibirsk 630090, Russia

[a)]**Author to whom correspondence should be addressed:** t.khabakhasheva@uea.ac.uk

ABSTRACT

The linear two-dimensional problem of flexural-gravity waves generated by an oscillating rigid plate build-in a floating poroelastic plate is studied. The problem is coupled. The plate deflections and the hydrodynamics loads are determined at the same time. The liquid under the poroelastic plate is inviscid and incompressible. Dynamics of the floating plate is described by a thin elastic plate equation. Porosity of the floating plate is taken into account only through the liquid flux into the plate. The velocity of the inflow is assumed to be governed by Darcy's law being proportional to the hydrodynamic pressure at the plate/liquid interface. Two cases of the oscillating rigid plate with and without its part in the liquid are considered. The problems are solved by the Fourier transform method for non-zero porosity and by the vertical mode method for elastic plates with zero porosity. The deflection and strain distributions are analyzed depending on the excitation frequency and the porosity. Two models of floating plate porosity, where the hydrostatic pressure is included into Darcy's law (Zavyalova's model) and excluded (Meylan's model), are compared. Plate porosity induces damping to the system. It is shown that the damping rate is non-monotonic with respect to the plate porosity.

I. INTRODUCTION

Interaction of water with porous floating or submerged structures is of interest in several applications. Porous structures are used in offshore and costal engineering to dissipate wave energy. Poroelastic models of sea ice become popular in polar engineering because such models are expected to explain attenuation energy of waves propagating through sea ice.

Sea ice is modeled as a thin poroelastic plate if the wavelength is much larger than the ice thickness. In many models, ice thickness is assumed constant. In this paper, we study the effect of a floating plate porosity on its response to a periodic in time external load. This response also depends on the excitation frequency and characteristics of the plate.

At equilibrium, the plate is at rest without any stresses in it. Pores extend from the plate/liquid interface to the upper dry surface of the plate. The level of the liquid inside the floating poroelastic plate depends on the plate thickness and density of the plate material. The applied external load deforms the plate, the liquid inside the plate moves, but the upper part of the plate always stays dry and the lower part of the plate always stay in contact with the liquid, which implies that the amplitude of the external load is relatively small and the problem can be approximately treated as linear. The liquid enters the plate pores if the plate moves downwards and/or the pressure at the plate/liquid interface increases. Correspondingly, the liquid exits from the pores then and there when and where the hydrodynamic pressure under the plate decreases.

The relation between the flux of the liquid into the pores and the local pressure is taken in the simplest form. It is assumed that the velocity of the liquid through the plate/liquid interface is proportional to the pressure gradient in the pores. Note that the pressure at the liquid interface inside the pores is equal to the atmospheric pressure. Other models of the liquid flow in the pores are possible, which account for capillary forces in the pores, presence of air in some closed pores, inertia effects, and more complex equations of liquid flows through the pores.

Models of submerged porous rigid and elastic plates are slightly different from the models of floating poroelastic plates. The liquid is on both sides of a submerged plate, and the hydrostatic pressure cannot move the liquid through the pores of the submerged plate. For a floating porous plate with pores being open to both surface of the plate,

a deviation of the hydrostatic pressure from its equilibrium initial value changes the liquid level inside the pore, this is, causes a flux of the liquid into the pores.

One of the first equations, which describe flows of a liquid through a porous body, is Darcy's law Darcy (1856). Darcy's law states that the flow flux between two points inside a porous body is proportional to the pressure drop over the distance between these points. The coefficient of the proportionality depends on the dynamic viscosity of the liquid μ and the permeability Π of the porous body. Scheidegger (1963) and Philip (1970) presented Darcy's law in the form

$$\vec{v} = -\frac{\Pi}{\mu}\nabla p, \tag{1}$$

where $\vec{v}$ is the flow velocity inside a porous body and ∇p is the pressure gradient. Equation (1) was discovered experimentally by Darcy but was derived later from the general equations of hydrodynamics. Darcy's law is a basic equation of hydrogeology.

Flows in porous media with high porosity are described by the Brickman equation

$$\nabla p = -\frac{\mu}{\Pi}\vec{v} + \mu_e \nabla^2 \vec{v}, \tag{2}$$

where μ_e is the so-called effective viscosity of the porous body. This equation generalizes Darcy's equation (1) including viscous stresses, see Saffman (1971) and Haber and Mauri (1983), for example. Sollitt and Cross (1972) and Ward (1964) demonstrated that the pressure gradient in large grain permeable media can be decomposed as

$$\nabla p = -\frac{\mu f}{\Pi}\vec{v} - \frac{C_f f^2 \rho}{\sqrt{\Pi}}|\vec{v}|\vec{v}, \tag{3}$$

where f is the porosity of the media, ρ is the fluid density, and C_f is a dimensionless turbulent resistance coefficient. Darcy's equation (1) is not applicable to high-speed flows, where it is replaced by the Forchheimer equation

$$-\nabla p = A\vec{v} + B|\vec{v}|\vec{v}, \tag{4}$$

where A and B are coefficients specific for the porous media, see Forchheimer (1901), Dagan (1989), and the review by Chwang and Chan (1998).

The wave propagating through porous elastic media with a compressible viscous fluid in the pores is described by the model developed by Biot (1956a and 1956b). Biot's model of saturated poroelastic media was used by Chen *et al.* (2019) to derive a dispersion relation for a floating poroelastic plate. Different forms of Darcy' law are used to study the interaction of porous structures with liquid. Not only equations describing flows in the porous structures but also the conditions on the liquid/structure interfaces can be specific for particular structures and interaction conditions.

The problem of gravity wave scattering by porous structures was investigated by many authors. Sollitt and Cross (1972) studied two-dimensional gravity wave reflection and transmission at permeable breakwaters of the rectangular cross section. They used linearized equation (3). The dispersion relation derived by Sollitt and Cross (1972) and the corresponding vertical models were investigated by McIver (1998) using the theory of non-self-adjoint differential operators. The corresponding three-dimensional problems with porous breakwaters were studied by Dalrymple *et al.* (1991).

Yu and Chwang (1994) used the boundary-element method (BEM) to study wave diffraction by a submerged horizontally porous plate. Matched eigenvalue function expansion methods were used in two-dimensional problems by Wu *et al.* (1998), Liu *et al.* (2008), Liu and Li(2011), Liu *et al.* (2012), and in three-dimensional problems by Chwang and Wu (1994), for example. With the help of the Wiener–Hopf technique, Evans and Peter (2011) obtained the formula for the reflection coefficient when a wave is obliquely incident upon a semi-infinite submerged porous plate. Cho and Kim (2013) and Cho *et al.* (2013) also used the eigenfunction expansion method to describe the interaction of oblique monochromatic incident waves with a submerged horizontal porous plate and to compare their result with a series of experiments. Gayen and Mondal (2014) reduced the problem of wave scattering by a porous plate to a second kind hypersingular integral equation in terms of the difference in the unknown velocity potential across the plate. This method is very powerful in submerged plate problems in two dimensions. The speed of the flow through the porous plate was governed be Darcy's law (1).

The studies listed above focused on flow interaction with the fixed porous plate without account for plate elasticity. In some cases, elasticity of the plate cannot be ignored, especially when porous structures are used to model sea ice in the polar regions. Wang and Ren (1993) studied reflection and transmission of small amplitude waves by a flexible porous and thin beam-like breakwater held fixed in the seabed. Wang and Ren (1994) studied wave trapping by a flexible porous barrier backed by an impermeable vertical end wall. Yip *et al.* (2002) investigated trapping of surface waves by submerged vertical porous flexible barriers near the end of a semi-infinitely long channel of finite depth and obtained the reflection coefficients for various wave conditions, geometrical settings, and barrier properties. Williams and Wang (2003) developed a new flexible porous wave barrier. The boundary integral equation method was applied in the flow domain. The dynamic behavior of the structure was investigated using an appropriate Green function. Predictions by the numerical model were confirmed by small-scale experiments. Kumar and Sahoo (2006) studied a flexible porous plate breakwater in a two-layer fluid. They considered the effects of both surface and internal waves and obtained the reflection and transmission coefficients for the surface and internal modes. Koley *et al.* (2015) reviewed calculation methods for wave scattering by a submerged vertical flexible porous plate in water of finite and infinite depths. Ashok *et al.* (2020) gave the analytical solution for the normally incident water wave scattering by a porous flexible vertical elastic plate in infinite water. More complicated problems with porous flexible plates were studied recently by Chanda and Bora (2021a), who considered two submerged porous barriers with different porosities, and by Luong and Nguyen (2023), who considered a perforated barrier with a quadratic pressure drop condition on it. Chanda and Bora (2021b) studied the combined effect of porous barriers and porous sea-bed on scattering of flexural-gravity waves. Wang *et al.* (2023) investigated flexural-gravity waves generated by a moving load with uniform current beneath the floating plate. Interaction of flexural-gravity waves with articulated plates was studied by Negi *et al.* (2023). Complex flows in the presence of porous bodies, viscoelastic plates, and broken ice were studied recently by Patari *et al.* (2023), Singh *et al.* (2023), Panduranga *et al.* (2023), and Ni *et al.* (2023).

Floating poroelastic plate models were used recently to simulate sea ice cover. Meylan *et al.* (2017) and Zheng *et al.* (2020c) developed

a poroelastic ice cover model using Eq. (1) without account for hydrostatic pressure, as it is the case for the submerged plate. They derived the corresponding dispersion relation and used it to extend the eigenfunction expansion method. A coupled boundary-element and finite-element method was also employed. The two methods provided the same results. They used both methods to calculate water-wave scattering by both a circular floating porous elastic plate and a porous elastic plate with arbitrary shape. They found that wave-energy dissipation due to the ice porosity initially increases as the plate becomes more porous, but reaches a maximum and then slowly decreases as the porosity increases further. The model by Meylan *et al.* (2017) can be used in the polar engineering field where porosity of the sea ice and dissipation of wave energy in ice are of concern. Zheng *et al.* (2020a) analyzed the hydroelastic interaction between water waves and multiple circular floating poroelastic plates and found that wave-power dissipation by the array of the plates is enhanced by the hydrodynamic interaction between the plates. Mohapatra *et al.* (2018) investigated the surface gravity wave interaction with the submerged flexible porous plate by using Green's function. Koley *et al.* (2018) investigated oblique surface gravity wave scattering by a floating flexible porous plate. By using Green's function, they converted the problem into a system of Fredholm type integral equations. It was observed that "quiet zones" exist for some angles of wave incidence. Smith *et al.* (2020) obtained the solution to the problem of water-wave scattering by a semi-infinite submerged thin porous or non-porous elastic plate by using the Wiener–Hopf technique.

Linear waves generated by a given external periodic load acting on a floating poroelastic plate were investigated by Zavyalova *et al.* (2021). In contrast to other models of poroelastic floating ice, they assumed that the speed of the flow into the floating plate is proportional to the total hydrodynamic pressure on the plate/liquid interface, including the hydrostatic pressure component.

In the present study, we investigate the difference between Meylan's model, see Meylan *et al.* (2017), without the hydrostatic pressure in Darcy's law and Zavyalova's model with the complete hydrodynamic pressure in Darcy's law for a two-dimensional problem with a floating poroelastic plate of infinite extent. Flexural-gravity waves in the plate are caused by a built-in rigid plate, and the angle of which with the vertical is a periodic function of time with a given frequency and amplitude. The rigid thin plate is either above the floating plate without any part of it under the plate or with a long submerged part extended down to the bottom. The first problem without submerged part of the rigid plate is formulated in Sec. II and solved in Sec. III within several approximations including the model of elastic floating plate with zero porosity. The second problem with a long part of the oscillating rigid plate in the liquid is studied in Sec. IV. We investigate the effect of the submerged part of the plate on the deflection of the floating poroelastic plate and strains in it within both Meylan's and Zavyalova's models in Sec. V. The observation from Meylan *et al.* (2017) that the wave dissipation is not a monotonic function of the floating plate porosity is confirmed and explained. The obtained numerical results and their discussions are presented in Sec. V. Finally, the conclusions are drawn in Sec. VI.

II. FORMULATION OF THE PROBLEM

Two-dimensional periodic in time deflection of a floating poroelastic plate is studied within the linear theory of hydroelasticity. The plate motion is caused by a rotation of a rigid plate build-in normally to the floating plate, see Fig. 1. In this section and in Sec. III, the rigid plate has no part in water below the floating plate. Therefore, the flow under the plate is caused by the floating plate deflection but not by the motion of the rigid plate directly. The problem with long submerged part of the rigid plate will be studied in Sec. IV.

The liquid under the floating plate is incompressible, inviscid, and of finite depth H. The problem is considered in the Cartesian coordinate system Oxy, where the line $y=0$ corresponds to the plate/liquid interface at equilibrium, the line $y=-H$ corresponds to the bottom of the liquid layer, and x is the horizontal coordinate with $x=0$ at the place where the rigid plate is built in the floating plate. The angle, $\Re(\theta e^{-i\omega t})$, of the rigid plate deviation from its equilibrium vertical position changes periodically in time t with a given frequency ω and small amplitude θ. Here, $\Re$ stands for the real part of a complex variable. The deflection of the poroelastic plate, $\Re[w(x)e^{-i\omega t}]$, is odd with respect to x, $w(-x)=-w(x)$. The flow caused by the deflection of the poroelastic plate is potential with a velocity potential $\Re[-i\omega\varphi(x,y)e^{-i\omega t}]$. The complex-valued functions to be determined, $\varphi(x,y)$ and $w(x)$, are proportional to θ within the linear theory of hydroelasticity. Without porosity of the floating plate, outgoing waves propagate in both directions from the place of excitation $x=0$. Porosity of the floating plate is responsible for damping of the generated waves and their decay with the distance from the place, where the plate excitation occurs. We shall determine the plate deflection and strains in the poroelastic plate depending on the frequency ω of excitation, elastic parameters of the floating plate, and its porosity. This problem is coupled. The hydrodynamic load acting on the floating plate and the plate deflection should be determined at the same time.

Within the linear theory of hydroelasticity, the complex amplitude of periodic plate deflection $w(x)$ is governed by the equation, see Squire *et al.* (1996)

$$-\omega^2 mw + D\frac{\partial^4 w}{\partial x^4} = p(x,0), \tag{5}$$

where m is the plate mass per unit area, $m=\rho_p h_p$, h_p is the plate thickness, ρ_p is the plate density, $D=Eh_p^3/[12(1-\nu^2)]$ is the plate rigidity, E is Young's modulus, ν is Poisson's ratio of the plate material, and $p(x,0)$ is the complex amplitude of the hydrodynamic pressure, $\Re(p(x,0)e^{-i\omega t})$, on the plate/liquid interface. The linearized Bernoulli equation provides

$$p(x,0)=\rho\omega^2\varphi(x,0)-\rho g w(x), \tag{6}$$

where ρ is the liquid density and g is the gravitational acceleration. Equations (5) and (6), as well as the following Eqs. (7) and (8), are

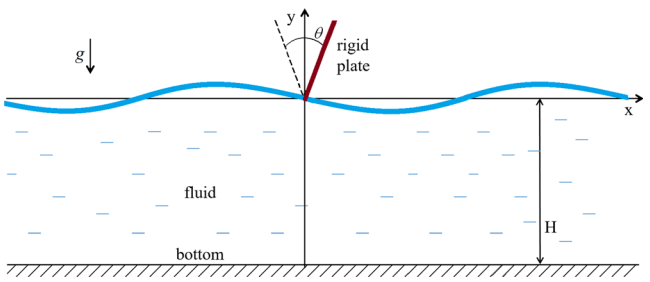

FIG. 1. Sketch of a rotating vertical plate in an poroelastic ice sheet.

obtained by separating time through $e^{-i\omega t}$ from the original time-periodic problem. The amplitude of the velocity potential $\varphi(x,y)$ satisfies Laplace's equation in the flow region and the bottom boundary condition

$$\begin{gathered}\varphi_{xx}+\varphi_{yy}=0 \quad (-H<y<0,-\infty<x<\infty),\\ \varphi_y=0 \quad (y=-H).\end{gathered} \tag{7}$$

The boundary condition on the surface of the poroelastic plate reads

$$\varphi_y(x,0)=w(x)+iv_n(x)/\omega, \quad v_n(x)=\varkappa p(x,0), \tag{8}$$

where $v_n(x)$ is the complex amplitude of the speed of the liquid penetrating the porous surface of the floating plate. This velocity is assumed to be proportional to the pressure on the plate/liquid interface with a coefficient $\varkappa$, see Zavyalova *et al.* (2021), where $\varkappa \geq 0$. The relation $v_n(x)=\varkappa p(x,0)$ comes from Darcy's law, see Darcy (1856), where the speed of the flow through a porous media, $v_n(x)$, is proportional to the gradient of the pressure, $p(x,0)/h_p$, with coefficient Π/μ. Here, Π is the vertical permeability of the plate, μ is the dynamic viscosity of the fluid, $\mu=1.8\times10^{-3}$ kg/(m s) for salt water, the pressure on the upper liquid surface inside the media is equal to the atmospheric pressure p_a, and the pressure on the plate/liquid interface is equal to $p(x,0)+p_a$. Then, $\varkappa=\Pi/(\mu h_p)$. Petrich *et al.* (2006) wrote about the sea ice permeability "Permeability is a function of the structure of the porous ice matrix, and the simplest way to parameterize this structure is through its brine volume fraction, i.e., the total porosity." Dependence of the sea ice permeability on ice porosity can be found in Freitag (1999) and Eicken *et al.* (2004). The experimental formula (40) from Eicken *et al.* (2004), see also Fig. 9 in Petrich *et al.* (2006), shows that the vertical permeability of sea ice varies from 10^{-13} to 10^{-10} m^2 when the total porosity changes from 0.1 to 0.4. The corresponding values of $\varkappa$ vary from 10^{-9} to 10^{-6} m^2 s/kg for ice plate of thickness 10 cm.

Note that the formula for $v_n(x)$ used in the analysis by Meylan *et al.* (2017) is different from (8). They accounted only for the dynamic pressure component in their analysis. This approach seems to come from the problems with submerged porous plates, where the hydrostatic pressures on both sides of the thin plate are equal and do not contribute to the flow through the plate. In the present problem with the floating porous plate, the upper surface of the plate is assumed to be dry with the atmospheric ambient pressure on the liquid surface inside the floating plate. We do not know at this stage which approach is right. To accommodate both approaches, we use the formula

$$v_n(x)=\varkappa\left[\rho\omega^2\varphi(x,0)-\delta\rho g w(x)\right],$$

where $\delta=0$ within the Meylan *et al.* (2017) model and $\delta=1$ within the Zavyalova *et al.* (2021) model.

The deflection $w(x)$ and the velocity potential $\varphi(x,y)$ decay as $x\to\pm\infty$ if $\varkappa>0$,

$$w(x)\to0, \quad \varphi(x,y)\to0 \quad (x\to\pm\infty). \tag{9}$$

It will be shown below that there is a special frequency, for which the outgoing wave exists for any porosity but only in the model with $\delta=1$. The functions $w(x)$ and $\varphi(x,y)$ describe outgoing waves for zero porosity, $\varkappa=0$.

The external excitation is described by the condition

$$w_x(\pm0)=\theta, \tag{10}$$

where θ is a given number. The condition (10) and Eqs. (5)–(9) imply that the plate deflection is odd function of x,

$$w(-x)=-w(x), \tag{11}$$

and, correspondingly, the flow is asymmetric

$$\varphi(-x,y)=-\varphi(x,y). \tag{12}$$

Equations (11) and (12) make it possible to consider the deflection and the flow only in $x>0$ with the following boundary conditions at $x=0$:

$$\varphi(0,y)=0 \quad (-H<y<0), \quad w(0)=0. \tag{13}$$

Note that the second, $w_{xx}(x)$, and the third, $w_{xxx}(x)$, derivatives are not necessarily continuous at $x=0$.

There are eight parameters, m, D, ρ, g, $\varkappa$, H, θ, ω, in the formulated problem. Within the linear approximation, the motion of the plate and the flow velocities are proportional to the amplitude θ of the external excitation. To minimize the number of parameters, it is convenient to introduce the following dimensionless variables:

$$\begin{gathered}x=H\tilde{x}, \quad y=H\tilde{y}, \quad w(x)=\theta H W(\tilde{x}),\\ \varphi(x,y)=\theta H^2\Phi(\tilde{x},\tilde{y}), \quad p(x,0)=\ \rho\, g\theta H P(\tilde{x}).\end{gathered} \tag{14}$$

Equations (5)–(13) in the dimensionless variables read

$$-æ\beta^2 W+\sigma\frac{\mathrm{d}^4W}{\mathrm{d}\tilde{x}^4}=P(\tilde{x}), \quad P(\tilde{x})=\beta^2\Phi-W(\tilde{x}) \quad (\tilde{x}>0), \tag{15}$$

$$\frac{\mathrm{d}W}{\mathrm{d}\tilde{x}}(0)=1, \quad W(0)=0, \quad W(\tilde{x})\to0 \quad (\tilde{x}\to\infty), \tag{16}$$

$$\begin{gathered}\frac{\partial^2\Phi}{\partial\tilde{x}^2}+\frac{\partial^2\Phi}{\partial\tilde{y}^2}=0 \quad (-1<\tilde{y}<0), \quad \frac{\partial\Phi}{\partial\tilde{y}}=0 \quad (\tilde{y}=-1),\\ \Phi(0,\tilde{y})=0 \quad (-1<\tilde{y}<0),\end{gathered} \tag{17}$$

$$\begin{gathered}\frac{\partial\Phi}{\partial\tilde{y}}=(1-i\gamma\delta)W+i\gamma\beta^2\Phi(0,\tilde{x}) \quad (\tilde{y}=0),\\ \Phi(\tilde{x},\tilde{y})\to0 \quad (\tilde{x}\to\infty).\end{gathered} \tag{18}$$

There are four dimensionless parameters in the problem (15)–(18)

$$æ=\frac{m}{\rho H}, \quad \beta=\omega\left(\frac{H}{g}\right)^{\frac{1}{2}}, \quad \sigma=\frac{D}{\rho g H^4}, \quad \gamma=\frac{\varkappa\rho g}{\omega}. \tag{19}$$

The dimensionless frequency β quantifies the importance of the dynamic effects compared with the bending of the plate and the hydrostatic pressure, where $H\omega^2$ is the acceleration scale of the flow. The problem (15)–(18) becomes decoupled for $\beta\ll1$. The parameter γ quantifies importance of the plate porosity. The floating plate is elastic but not porous if $\gamma=0$. The plate porosity is more important for low frequencies ω and is negligible for high frequencies of excitation. The parameter æ is the ratio of the structural mass m and the product ρH, which is of the order of the added mass of the floating plate per unit area. For a floating plate we have $\rho_p<\rho$, and the plate thickness h_p is smaller than H in the thin plate approximation (5). Therefore, in practical problems, æ <1. The parameter σ indicates importance of

bending stresses compared with the hydrostatic pressure under the plate. Depending on values of these four parameters, different models of floating poroelastic plate behavior can be derived.

The complex amplitude $\varepsilon(\tilde{x})$ of the strains in the floating plate is related to the dimensionless deflection $W(\tilde{x})$ by the formula

$$\varepsilon(\tilde{x}) = \varepsilon_{sc}\frac{\mathrm{d}^2 W}{\mathrm{d}\tilde{x}^2}, \quad \varepsilon_{sc} = \frac{h_p\theta}{2H}, \tag{20}$$

where ε_{sc} is the scale of the strains.

The dimensionless parameter PH, which describes porosity in the paper by Meylan *et al.* (2017), is related to the parameters (19) by the formula $PH = \beta^2\gamma$. For α in the range from 10^{-9} to 10^{-6} m^2 s/kg, the parameter γ is in the range from 10^{-5} to 10^{-2} s$^{-1}/\omega$ for a sea-ice plate of thickness 10 cm.

III. APPROXIMATE SOLUTIONS OF THE COUPLED PROBLEM FOR POROELASTIC PLATE

Approximate solutions of the problem (11)–(15), which are valid for different limiting values of the parameters (15), as well as the complete solution of the original problem, are derived in this section. These solutions will be used for analysis of poroelastic plate behavior in Sec. V. As a reference case, we select the problem without presence of the liquid under the plate, when the plate porosity does not matter. Then, we find asymptotic solution for low-frequency excitation and the complete solution using the Fourier transform. Finally, the problem of floating elastic plate without porosity is solved using the so-called vertical modes.

A. Periodic excitation of a dry plate

We start with the simplest model of dry plate, where the right-hand side of the plate equation (15) is zero. The solution of the homogeneous equation (15) with the boundary conditions (16), which describes elastic waves propagating to infinity from the excitation place, $\tilde{x} = 0$, will be determined analytically.

The deflection of the dry plate, which is denoted by $W_d(\tilde{x})$, satisfies the following equations:

$$\begin{gathered}\sigma\frac{\mathrm{d}^4 W_d}{\partial\tilde{x}^4} = æ\beta^2 W_d \quad (\tilde{x} > 0), \quad \frac{\mathrm{d}W_d}{\partial\tilde{x}}(0) = 1,\\ W_d(0) = 0, \quad W_d(\tilde{x}) \sim ae^{i\lambda\tilde{x}} \ (\tilde{x} \to +\infty),\end{gathered} \tag{21}$$

where a is a complex amplitude of the outgoing wave to be determined and $\lambda = (æ\beta^2/\sigma)^{\frac{1}{4}}$ is the dimensionless wave number of the outgoing wave.

A general solution of the problem (21) which satisfies the far-field condition as $x \to \infty$ reads

$$W_d(\tilde{x}) = ae^{i\lambda\tilde{x}} + be^{-\lambda\tilde{x}}, \tag{22}$$

where the coefficients a and b are determined using the boundary conditions at $\tilde{x} = 0$,

$$a = \frac{1}{2\lambda}(1-i) = \frac{1}{\lambda\sqrt{2}}e^{-i\pi/4}, \quad b = -a. \tag{23}$$

The resulting amplitude of the dry plate deflection is given by

$$|W_d(\tilde{x})| = \frac{1}{\lambda\sqrt{2}}[1 - 2e^{-\lambda\tilde{x}}\cos\lambda\tilde{x} + e^{-2\lambda\tilde{x}}]^{\frac{1}{2}}, \tag{24}$$

and the amplitude of the strains $|\varepsilon_d|$ along the dry plate follows from (20) as:

$$|\varepsilon_d(\tilde{x})| = \varepsilon_{sc}\frac{\lambda}{\sqrt{2}}[1 + 2e^{-\lambda\tilde{x}}\cos\lambda\tilde{x} + e^{-2\lambda\tilde{x}}]^{\frac{1}{2}}. \tag{25}$$

The maximum of the strains in the plate, $|\varepsilon|_{\max} = \sqrt{2}\lambda\,\varepsilon_{sc}$, is achieved at $x = 0$. The strain in the far field, where $x \to +\infty$, is twice smaller than at the excitation place, $x = 0$.

B. Low-frequency limit

In this section, we investigate the floating plate deflection, $W_l(\tilde{x})$, for low frequency, $\beta \ll 1$, of the excitation using methods of asymptotic analysis. The solution of the problem (15)–(18) in the limit as $\beta^2 \to 0$ is sought in the form

$$\begin{aligned}W_l(\tilde{x}) &= W_0(\tilde{x}) + \beta^2 W_1(\tilde{x}) + O(\beta^4),\\ \Phi_l(\tilde{x},\tilde{y}) &= \Phi_0(\tilde{x},\tilde{y}) + \beta^2\Phi_1(\tilde{x},\tilde{y}) + O(\beta^4).\end{aligned} \tag{26}$$

The subscript l stands for the low-frequency approximation.

In the leading order, the problem is decoupled. Only the hydrostatic pressure matters. The zero order plate deflection $W_0(\tilde{x})$ is governed by the equations

$$\sigma\frac{\mathrm{d}^4 W_0}{\mathrm{d}\tilde{x}^4}(0) = -W_0, \quad (\tilde{x} > 0), \quad \frac{\mathrm{d}W_0}{\mathrm{d}\tilde{x}}(0) = 1, \quad W_0(0) = 0. \tag{27}$$

The bounded solution of (27) reads

$$W_0(\tilde{x}) = \frac{\sqrt{2}}{\tau}e^{-\tau\tilde{x}/\sqrt{2}}\sin\left(\tau\tilde{x}/\sqrt{2}\right), \tag{28}$$

where $\tau = \sqrt[4]{1/\sigma}$. The solution $W_0(\tilde{x})$ decays exponentially with the distance from the excitation place, $\tilde{x} = 0$. There are no outgoing waves in the limit of small frequencies. The maximum dimensionless deflection $|W_{0,\max}| = \sqrt{2}\tau^{-1}e^{-\pi/4}$ is achieved at $x = \sqrt{2}\pi/(4\tau)$. The maximum strain is achieved at $\tilde{x} = 0$ and is equal to $\sqrt{2}\tau\varepsilon_{sc}$.

The leading order velocity potential $\Phi_0(\tilde{x},\tilde{y})$ is governed by the equations

$$\begin{gathered}\frac{\partial^2\Phi_0}{\partial\tilde{x}^2} + \frac{\partial^2\Phi_0}{\partial\tilde{y}^2} = 0 \quad (-1 < \tilde{y} < 0), \quad \frac{\partial\Phi_0}{\partial\tilde{y}} = 0 \quad (\tilde{y} = -1),\\ \frac{\partial\Phi_0}{\partial\tilde{y}} = (1 - i\gamma\delta)W_0(\tilde{x}) \quad (\tilde{y} = 0),\end{gathered} \tag{29}$$

$$\Phi_0(0,\tilde{y}) = 0 \quad (-1 < \tilde{y} < 0), \quad \Phi_0(\tilde{x},\tilde{y}) \to 0 \quad (\tilde{x} \to \infty). \tag{30}$$

The problem (29) and (30) is solved by using the sine Fourier transform

$$\begin{aligned}\Phi^s(\xi,\tilde{y}) &= \int_0^\infty \Phi(\tilde{x},\tilde{y})\sin(\xi\tilde{x})\mathrm{d}\hat{\tilde{x}},\\ \Phi(\tilde{x},\tilde{y}) &= \frac{2}{\pi}\int_0^\infty \Phi^s(\xi,\tilde{y})\sin(\xi\tilde{x})\mathrm{d}\xi.\end{aligned} \tag{31}$$

Applying the transform (31) to the equations and boundary conditions in (29) and (30), we obtain

$$\Phi_0^s(\xi,\tilde{y}) = \frac{(1-i\gamma\delta)\cosh[\xi(y+1)]W_0^s(\xi)}{\xi\sinh(\xi)}, \tag{32}$$

where $W_0^s(\xi)$ is a sine Fourier transform of $W_0(\tilde{x})$,

$$W_0^s(\xi) = \int_0^\infty W_0(\tilde{x})\sin(\xi\tilde{x})\mathrm{d}\tilde{x}, \quad W_0(\tilde{x}) = \frac{2}{\pi}\int_0^\infty W_0^s(\xi)\sin(\xi\tilde{x})\mathrm{d}\xi. \tag{33}$$

The solution (28) provides

$$W_0^s(\xi) = \frac{\sqrt{2}\tau\sigma\xi}{\sigma\xi^4+1}. \tag{34}$$

Then,

$$\Phi_0^s(\xi,\tilde{y}) = \frac{\sqrt{2}\sigma\tau(1-i\gamma\delta)\cosh[\xi(\tilde{y}+1)]}{(\sigma\xi^4+1)\sinh(\xi)}. \tag{35}$$

The problem for the first-order plate deflection $W_1(\tilde{x})$ is obtained by substituting (26) in (15), (16) and collecting terms of order $O(\beta^2)$,

$$\sigma\frac{\mathrm{d}^4W_1}{\mathrm{d}\tilde{x}^4}(0) + W_1 = \Phi_0(\tilde{x},0) + æW_0 \quad (\tilde{x}>0), \qquad \frac{\mathrm{d}W_1}{\mathrm{d}\tilde{x}}(0) = 0, \quad W_1(0) = 0. \tag{36}$$

The sine transform (33) applied to (36) and the leading order solutions (34) and (32) provide

$$W_1^s(\xi) = -\frac{\sigma\xi}{\sigma\xi^4+1}W_1'(0) + \sqrt{2}æ\tau\frac{\sigma\xi}{(\sigma\xi^4+1)^2} + \frac{\sqrt{2}\sigma\tau(1-i\gamma\delta)}{(\sigma\xi^4+1)^2\tanh(\xi)}. \tag{37}$$

The derivative $W_1'(0)$ in (37) is determined using the condition

$$\frac{\mathrm{d}W_1}{\mathrm{d}\tilde{x}}(0) = \frac{2}{\pi}\int_0^\infty W_1^s(\xi)\xi\mathrm{d}\xi = 0. \tag{38}$$

Once $W_1'(0)$ has been determined, $W_1(\tilde{x})$ is calculated by applying the inverse transform (33)–(37). It is seen that for small β, the inertia of plate and the hydrodynamic pressure acting on the plate can be ignored at the leading order, only the elastic force and the hydrostatic pressure govern the motion of the floating poroelastic plate.

C. Original hydroelastic problem

The solution of the original problem (15)–(18) is obtained using the sine Fourier transform (33) and (31). Applying this transform to Eqs. (15)–(18) and denoting the corresponding deflection by $W_u(\tilde{x})$, we find

$$-æ\beta^2W_u^s(\xi) + \sigma\left[\xi^4W_u^s(\xi) + \xi W_u''(0)\right] = \beta^2\Phi^s(\xi,0) - W_u^s(\xi), \tag{39}$$

$$\frac{\partial^2\Phi_u^s(\xi,\tilde{y})}{\partial\tilde{y}^2} - \xi^2\Phi_u^s(\xi,\tilde{y}) = 0\,(-1<\tilde{y}<0), \qquad \frac{\partial\Phi_u^s(\xi,\tilde{y})}{\partial\tilde{y}} = 0\,(\tilde{y}=-1), \tag{40}$$

$$\frac{\partial\Phi_u^s}{\partial\tilde{y}} = (1-i\gamma\delta)W_u^s(\xi) + i\gamma\beta^2\Phi_u^s(\xi,0)\,(\tilde{y}=0). \tag{41}$$

The solution of Eqs. (39)–(41) reads

$$W_u^s(\xi) = -\sigma W_u''(0)F(\xi), \qquad F(\xi) = \frac{\xi(\xi\tanh(\xi) - i\gamma\beta^2)}{(\sigma\xi^4+1-æ\beta^2)(\xi\tanh(\xi)-i\gamma\beta^2) - \beta^2(1-i\gamma\delta)}. \tag{42}$$

The derivative $W_u''(0)$ is determined using the first condition in (16)

$$\frac{\mathrm{d}W_u}{\mathrm{d}\tilde{x}}(0) = \frac{2}{\pi}\int_0^\infty W_u^s(\xi)\xi\mathrm{d}\xi = -\frac{2}{\pi}\sigma W_u''(0)\int_0^\infty F(\xi)\xi\mathrm{d}\xi = 1. \tag{43}$$

The function $F(\xi)$ behaves as $O(\xi^{-3})$ for $\xi\to\infty$. To improve the convergence of the integrals in the inverse Fourier transforms, the function $F(\xi)$ is decomposed as

$$F(\xi) = \frac{\xi}{\sigma\xi^4+1} + F_1(\xi), \tag{44}$$

where $F_1(\xi)$ behaves as $O(\xi^{-8})$ for $\xi\to\infty$. Then, the plate deflection can be written as

$$W_u(\tilde{x}) = -\frac{2}{\pi}\sigma W_u''(0)\left\{\frac{\pi\tau^2}{2}e^{-\tau\tilde{x}/\sqrt{2}}\sin\left(\tau\tilde{x}/\sqrt{2}\right) + \int_0^\infty F_1(\xi)\sin(\xi\tilde{x})\mathrm{d}\xi\right\}, \tag{45}$$

where $\tau = \sqrt[4]{1/\sigma}$. Compare the first term in (45) with the leading order solution (28) for small frequencies. The integral in (45) converges quickly, because the function $F_1(\xi)$ is bounded and decays as $O(\xi^{-8})$ for $\xi\to\infty$.

The strains $\varepsilon_u(\tilde{x})$ defined in (20) are given by the formula

$$\varepsilon_u(\tilde{x}) = \frac{2}{\pi}\sigma W_u''(0)\varepsilon_{sc}\left\{\frac{\pi\tau^4}{2}e^{-\tau\tilde{x}/\sqrt{2}}\cos\left(\tau\tilde{x}/\sqrt{2}\right) + \int_0^\infty \xi^2F_1(\xi)\sin(\xi\tilde{x})\mathrm{d}\xi\right\}. \tag{46}$$

The integral in (46) converges quickly because $\xi^2F_1(\xi)$ behaves as $O(\xi^{-6})$ for $\xi\to\infty$.

The solution (45) and (46) cannot be used if the denominator, $R(\xi) = (\sigma\xi^4+1-æ\beta^2)\xi\tanh(\xi) - \beta^2 - i\gamma\beta^2(\sigma\xi^4 \quad +1-æ\beta^2-\delta)$, of the function $F(\xi)$ defined in (42) is zero for a real positive ξ. There is a real root of the equation $R(\xi)=0$ for zero porosity, $\gamma=0$. This case is considered in Sec. III D. The equation $R(\xi)=0$ has no real roots if $\gamma\neq0$ and $\delta=0$, which is within the Meylan model. However, for $\gamma\neq0$ and $\delta=1$ the equation $R(\xi)=0$ has a real root ξ^*, which is independent of the porosity parameter γ. The dimensionless wave number ξ^* is the solution of the equation $\tanh\xi^* = \sigma\xi^{*3}/æ$ for the dimensionless frequency $\beta = \xi^{*2}\sqrt{\sigma/æ}$. Therefore, Zavyalova's model with $\delta=1$ predicts a wave propagating from the excitation place for any porosity. This finding makes the Meylan's and Zavyalova's models different despite the fact that the parameter δ appears in the solution only through the product $\gamma\delta$ which is small for practical values of the porosity parameter α.

D. Hydroelastic problem with zero porosity

For $\gamma=0$, the problem (15)–(18) is that of forced flexural-gravity waves. Excitation of floating elastic plate produces waves outgoing to infinity. The deflection of the elastic plate, which is denoted by $W_v(\tilde{x})$,

does not decay at $x=+\infty$. Correspondingly, the sine transform (33) cannot be used directly to solve the problem (15)–(18) with $\gamma=0$. However, the transform (33) can be used if one separates the wave part of the deflection from the formulation as it was done in Brocklehurst *et al.* (2010). Another approach, which will be used below, is based on the method of vertical modes, Korobkin *et al.* (2019) and Wu *et al.* (2023).

The vertical modes are the functions of the vertical coordinate $\tilde{y}$,

$$f_n(\tilde{y}) = \frac{\cosh[\kappa_n(\tilde{y}+1)]}{\kappa_n \sinh[\kappa_n]}, \tag{47}$$

where κ_n, $n=-2,-1,0,1,2,\ldots$ are complex solutions of the dispersion relation $(\kappa^4+\mu)\kappa\tanh\kappa = q$, $q=\beta^2/\sigma$, and $\mu = 1/\sigma - æq$, see Wu *et al.* (2023) for more details. The vertical modes are orthogonal

$$\langle f_n(\tilde{y}), f_m(\tilde{y})\rangle = 0 \quad (n\neq m), \quad \langle f_n(\tilde{y}), f_n(\tilde{y})\rangle = Q_n \quad (n\geq -2), \tag{48}$$

where the scalar product is given by

$$\langle G_1(\tilde{y}), G_2(\tilde{y})\rangle = \int_{-1}^{0} G_1(\tilde{y})G_2(\tilde{y})\,\mathrm{d}\tilde{y} + \frac{1}{q}(G_1'''(0)G_2'(0) + G_1'(0)G_1'''(0)), \tag{49}$$

for any functions $G_1(\tilde{y})$ and $G_2(\tilde{y})$ defined in $-1<\tilde{y}<0$, and

$$Q_n = \frac{1}{2\kappa_n^2 q^2}\left[(\kappa_n^4+\mu)^2\kappa_n^2 + q(5\kappa_n^4+\mu-q)\right]. \tag{50}$$

The generalized orthogonality relations (48), where the scalar product is given by (49), were originally derived by Sahoo *et al.* (2001) and subsequently by Manam *et al.* (2006).

The products $e^{i\kappa_n\tilde{x}}f_n(\tilde{y})$, $n\geq -2$, satisfy Laplace's equation and describe waves propagating toward $x=+\infty$ for $n=0$. A general solution of the boundary-value problem (15)–(18) reads

$$\Phi_v(\tilde{x},\tilde{y}) = \sum_{n=-2}^{\infty} A_n^v e^{i\kappa_n\tilde{x}} f_n(\tilde{y}), \quad W_v(\tilde{x}) = \sum_{n=-2}^{\infty} A_n^v e^{i\kappa_n\tilde{x}}, \tag{51}$$

with undetermined complex coefficients A_n^v.

To find the coefficients A_n^v, the following limits, where $n\geq -2$, are calculated in two ways, by using (51) and (49):

$$\lim_{x\to 0}\langle \Phi_v(\tilde{x},\tilde{y}), f_n(\tilde{y})\rangle = A_n^v Q_n, \tag{52}$$

and using (47) and (16), and the third condition in (17)

$$\lim_{\tilde{x}\to 0}\langle \Phi^v(\tilde{x},\tilde{y}), f_n(\tilde{y})\rangle = -W_v''(0)/q. \tag{53}$$

Equating (52) and (53), and using the series (51), we obtain the deflection of the elastic plate

$$W_v(\tilde{x}) = -\frac{W_v''(0)}{q}\sum_{n=-2}^{\infty}\frac{e^{i\kappa_n\tilde{x}}}{Q_n}, \tag{54}$$

where the second derivative $W_v''(0)$ is determined by the condition, see (16), $W'(0)=1$, as

$$W_v''(0) = iq\left(\sum_{n=-2}^{\infty}\frac{\kappa_n}{Q_n}\right)^{-1}. \tag{55}$$

The amplitude of the flexural-gravity wave at infinity, $x\to+\infty$, is equal to A_0^v. The solution (55) and (54) without porosity will be compared with the solution (45), where the porosity parameter γ is small, to establish conditions where the plate porosity plays a negligible role.

IV. LONG RIGID PLATE PROBLEM

In Secs. II and III, the built-in rigid plate was only above the floating plate without its submerged part. The effect of the submerged part of the rigid rotating plate on the deflection of the floating plate could be strong for certain ranges of frequencies and porosity. Only the problem with long submerged part of the rigid plate extended down to the bottom is considered here, see Fig. 2. The motion of the plate directly drives the motion of the water now. The plate deflection and the corresponding velocity potential are denoted by $W_s(\tilde{x})$ and $\Phi_s(\tilde{x},\tilde{y})$ where s stands for "rotating rigid plate with long *submerged* part."

A. Poroelastic floating plate

The functions $W_s(\tilde{x})$ and $\Phi_s(\tilde{x},\tilde{y})$ are odd with respect to the horizontal coordinate $\tilde{x}$. They satisfy the same equations and conditions as for the rigid plate without a submerged part, (15)–(18), but now the velocity potential is no longer continuous at $\tilde{x}=0$ and the third condition in (17) should be replaced by the body boundary condition on the submerged part of the rotating rigid plate

$$\frac{\partial\Phi_s(0,\tilde{y})}{\partial\tilde{x}} = -\tilde{y} \quad (-1<\tilde{y}<0). \tag{56}$$

The cosine Fourier transform,

$$\Phi_s^c(\xi,\tilde{y}) = \int_0^{\infty}\Phi_s(\tilde{x},\tilde{y})\cos(\xi\tilde{x})\mathrm{d}\tilde{x}, \qquad \Phi_s(\tilde{x},\tilde{y}) = \frac{2}{\pi}\int_0^{\infty}\Phi_s^c(\xi,\tilde{y})\cos(\xi\tilde{x})\mathrm{d}\xi, \tag{57}$$

is applied to Laplace's equation and the bottom condition with the result

$$\frac{\partial^2\Phi_s^c}{\partial\tilde{y}^2}(0,\tilde{y}) - \xi^2\Phi_s^c(0,\tilde{y}) = -\tilde{y}, \quad \frac{\partial\Phi_s^c}{\partial\tilde{y}}(\xi,-1) = 0. \tag{58}$$

A general solution of the problem (58) reads

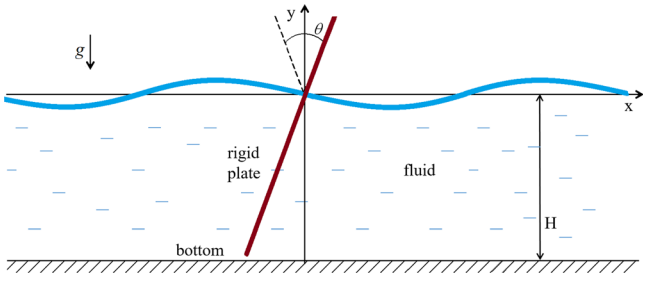

FIG. 2. Sketch of a floating poroelastic plate with a built-in rotating vertical plate having a long submerged part.

$$\Phi_s^c(\xi,\tilde{y}) = C_c(\xi)\cosh[\xi(\tilde{y}+1)] - \frac{1}{\xi^3}\sinh[\xi(\tilde{y}+1)] + \frac{\tilde{y}}{\xi^2}, \quad (59)$$

where $C_c(\xi)$ is to be determined. Applying (57) and cosine Fourier transform for $W_s(\tilde{x})$

$$W_s^c(\xi) = \int_0^\infty W_s(\tilde{x})\cos(\xi\tilde{x})\mathrm{d}\tilde{x}, \quad W_s(\tilde{x}) = \frac{2}{\pi}\int_0^\infty W_s^c(\xi)\cos(\xi\tilde{x})\mathrm{d}\xi, \quad (60)$$

to the plate equation (15) and the condition on the plate/liquid interface (18), and using (59), we find

$$W_s^c(\xi) = W_s'''(0)\left[\frac{1}{\xi^4+\tau^4} + \frac{\sigma F_1(\xi)}{\xi}\right] - \frac{\xi^2}{\xi^4+\tau^4} - \sigma\xi F_1(\xi) - \frac{\cosh\xi - 1}{\xi^2\cosh\xi}\frac{\beta^2 F(\xi)}{\xi(\xi\tanh(\xi) - i\gamma\beta^2)}, \quad (61)$$

where $F(\xi)$ is introduced in (42) and $F_1(\xi)$ in (44). The terms in (61) behave as $O(\xi^{-4})$, $O(\xi^{-9})$, $O(\xi^{-2})$, $O(\xi^{-7})$, and $O(\xi^{-7})$, correspondingly. The inverse Fourier transforms of the first and third terms are obtained by using table integrals, see Gradshteyn and Ryzhik (2014), formulas 3.723. 1 and 7

$$\int_0^\infty \frac{\cos(\xi\tilde{x})}{\xi^4+\tau^4}\mathrm{d}\xi = \frac{\pi\sqrt{2}}{4\tau^3}e^{-\tau\tilde{x}/\sqrt{2}}\left[\cos\left(\tau\tilde{x}/\sqrt{2}\right) + \sin\left(\tau\tilde{x}/\sqrt{2}\right)\right], \quad (62)$$

$$\int_0^\infty \frac{\xi^2\cos(\xi\tilde{x})}{\xi^4+\tau^4}\mathrm{d}\xi = \frac{\pi\sqrt{2}}{4\tau}e^{-\tau\tilde{x}/\sqrt{2}}\left[\cos\left(\tau\tilde{x}/\sqrt{2}\right) - \sin\left(\tau\tilde{x}/\sqrt{2}\right)\right]. \quad (63)$$

Note that the integral (63) behaves as $\pi\sqrt{2}/(4\tau) - (\pi/2)\tilde{x} + O(\tilde{x}^2)$ $\tilde{x}\to 0$, which together with (61) proves that the edge condition $W_s'(0) = 1$ is satisfied.

The second edge condition $W_s(0) = 0$, the inverse Fourier transform (60), and the solution (61) lead to the equation for the derivative $W_s'''(0)$,

$$W_s'''(0)\left[\frac{\pi\sqrt{2}}{4\tau^3} + \sigma\int_0^\infty \frac{1}{\xi}F_1(\xi)\,\mathrm{d}\xi\right] = \frac{\pi\sqrt{2}}{4\tau} + \int_0^\infty (\sigma\xi F_1(\xi) + \frac{\beta^2 F(\xi)(\cosh\xi - 1)}{\xi^3(\xi\tanh(\xi) - i\gamma\beta^2)\cosh\xi})\mathrm{d}\xi. \quad (64)$$

The integrals in (64) quickly converge. The deflection is given as

$$W_s(\tilde{x}) = \frac{e^{-\tau\tilde{x}/\sqrt{2}}}{\sqrt{2}\tau^3}\left[(W_s'''(0) - \tau^2)\cos\left(\tau\tilde{x}/\sqrt{2}\right) + (W_s'''(0) + \tau^2)\sin\left(\tau\tilde{x}/\sqrt{2}\right)\right] + \frac{2}{\pi}\int_0^\infty (W'''_s(0)\frac{\sigma F_1(\xi)}{\xi} - \sigma\xi F_1(\xi) - \frac{\beta^2 F(\xi)(\cosh\xi - 1)}{\xi^3(\xi\tanh(\xi) - i\gamma\beta^2)\cosh\xi})\cos(\xi\tilde{x})\mathrm{d}\xi, \quad (65)$$

where the integral quickly converges.

The strain distribution (20) follows from (65) as

$$\varepsilon_s(\tilde{x})/\varepsilon_{sc} = \frac{e^{-\tau\tilde{x}/\sqrt{2}}}{\sqrt{2}\tau}\left[(W_s'''(0) - \tau^2)\sin\left(\tau\tilde{x}/\sqrt{2}\right) - (W_s'''(0) + \tau^2)\cos\left(\tau\tilde{x}/\sqrt{2}\right)\right] - \frac{2}{\pi}\int_0^\infty (W'''_s(0)\frac{\sigma F_1(\xi)}{\xi} - \sigma\xi F_1(\xi) - \frac{\beta^2 F(\xi)(\cosh\xi - 1)}{\xi^3(\xi\tanh(\xi) - i\gamma\beta^2)\cosh\xi})\xi^2\cos(\xi\tilde{x})\mathrm{d}\xi. \quad (66)$$

B. Elastic floating plate

Similar to Sec. III D, the vertical mode method is used to find deflections and strains for an elastic floating plate with built-in vertical long rigid plate. The complex amplitudes of the deflection and velocity potential are denoted by $W_z(\tilde{x})$ and $\Phi_z(\tilde{x},\tilde{y})$ correspondingly. Note that the subscript z does not mean "partial derivative with respect to z" here but stands for "*zero* porosity."

The vertical modes $f_n(\tilde{y})$, the definition of the scalar product (49), and the orthogonality condition (48) are the same as in Sec. III D for a vertical rigid plate without submerged part.

A general solution of the boundary-value problem (15)–(18), where the boundary condition at $\tilde{x} = 0$ is changed for (56) in the problem with the long rigid plate, can be written in the form similar to (51)

$$\Phi_z(\tilde{x},\tilde{y}) = \sum_{n=-2}^{\infty} A_n^z e^{i\kappa_n\tilde{x}} f_n(\tilde{y}), \quad W_z(\tilde{x}) = \sum_{n=-2}^{\infty} A_n^z e^{i\kappa_n\tilde{x}}, \quad (67)$$

with undetermined complex coefficients A_n^z.

To find the coefficients A_n^z, the following limits where $n \geq -2$, are calculated in two ways, by using (67) and (49):

$$\lim_{\tilde{x}\to 0}\left\langle \frac{\partial\Phi_z(\tilde{x},\tilde{y})}{\partial\tilde{x}}, f_n(\tilde{y})\right\rangle = i\kappa_n A_n^z Q_n, \quad (68)$$

and

$$\lim_{\tilde{x}\to 0}\left\langle \frac{\partial\Phi_z(\tilde{x},\tilde{y})}{\partial\tilde{x}}, f_n(\tilde{y})\right\rangle = T_n - \frac{1}{q}W'''(0), \quad T_n = -\int_{-1}^{0}\tilde{y}f_n(\tilde{y})\,\mathrm{d}\tilde{y} + \frac{\kappa_n^2}{q}. \quad (69)$$

Equating (68) and (69), we obtain

$$A_n^z = \frac{T_n}{i\kappa_n Q_n} - \frac{W_z'''(0)}{qi\kappa_n Q_n}. \quad (70)$$

The condition $W_z(0) = 0$, the series (67) and the formula (70), provides the third derivative $W_z'''(0)$ as

$$W_z'''(0) = q\sum_{n=-2}^{\infty}\frac{T_n}{k_n Q_n}\left(\sum_{n=-2}^{\infty}\frac{1}{k_n Q_n}\right)^{-1}. \quad (71)$$

It was confirmed numerically that the second condition, $W_z'(0) = 1$, is satisfied with the series (67) and formulas (70) and (71).

The series in (71) and the series for the deflection (67) together with its second derivative $W_z''(\tilde{x})$ required for calculations of the strain

distribution in the floating plate converge quickly because $Q_n = O(n^8)$ when $n \to \infty$, see Korobkin *et al.* (2019).

V. NUMERICAL RESULTS

Deflections and strains predicted by the models from Secs. III and IV are calculated and analyzed for an ice plate with different porosity excited by a built-in thin rigid plate at different frequencies. The obtained solutions are compared one with another to understand the damping mechanism of the porosity. It will be shown that damping of the generated waves is not proportional to porosity of the floating plate.

Calculations are performed for the following characteristics of the problem: gravitational acceleration $g = 9.8$ m/s^2, density of the plate material $\rho_i = 917$ kg/m^3, plate thickness $h_p = 1$ m, Young's modulus of the floating plate material $E = 4.2 \times 10^9$ N/m^2, and Poisson's ratio of the plate material $\nu = 0.33$. Hence, the flexural rigidity of the floating plate is $D = 3.92 \times 10^8$ N m, and the mass of the floating plate per unit area is equal to $m = 917$ kg/m^2. The water density is $\rho = 1025$ kg/m^3, and the water depth is $H = 10$ m. The corresponding values of the dimensionless parameters are $\sigma = 3.9$ and $æ = 0.09$. The scale of the angular frequency, $\sqrt{H/g}$, is equal to 1.01, which shows that the value of the dimensionless frequency β is approximately equal to the value of the frequency ω in seconds. The dimensionless frequency β varies in our calculations from 0.001 to 5.05. The values of the porosity parameter α are estimated for ice plate in Sec. II. For the ice plate of thickness 1 m, these estimates give the range of α from 10^{-10} to 10^{-7} m^2 s/kg. Then, the parameter γ varies from 2×10^{-6} to 1. In our analysis, we consider a wider range of γ to investigate the effect of the floating plate porosity on plate deflection and strains in the plate.

The series and integrals in the formulas for different solutions converge quickly enough for accurate calculations. The function $F_1(\xi)$ in (45) decays as $O(\xi^{-8})$ for $\xi \to \infty$. Correspondingly, the integral in (46) converges quickly because $\xi^2 F_1(\xi) = O(\xi^{-6})$ as $\xi \to \infty$. The series in (54) and (55) converge quickly because their terms decay as $O(n^{-8})$ and $O(n^{-7})$ for $n \to \infty$, accordingly. The series (67) for the deflection and (71) for the third derivative of the deflection at $\tilde{x} = 0$ converge quickly because their terms decay at least as $O(n^{-7})$ for $n \to \infty$.

For a rigid plate without submerged part, the dimensionless amplitudes, $|W(\tilde{x})|$, of the floating plate deflection as functions of the dimensionless distance $\tilde{x}$ along the plate from the excitation place, $\tilde{x} = 0$, are shown in Fig. 3 for different dimensionless frequencies β with account for porosity with $\alpha = 10^{-4}$ m^2 s/kg. In this figure, we compare the amplitudes of the complete deflection $|W_u(\tilde{x})|$ given in Eq. (45) and shown by red lines and the deflection $|W_l(\tilde{x})|$ predicted by the low-frequency approximation (26) with two terms (dashed lines) and with the leading approximation $|W_0(\tilde{x})|$ only, see Eq. (28) (blue lines). The leading order low-frequency deflection $|W_0(\tilde{x})|$ approximates the complete deflection $|W_u(\tilde{x})|$ with a good accuracy for $\beta = 0.001$. The two-term approximation (26) can be used for wider range of the frequencies.

The relative difference between the complete deflection (45) and the two-term low-frequency approximation (26), $100\%(|W_u(\tilde{x})| - |W_l(\tilde{x})|)/|W_u(\tilde{x})|$, is shown in Fig. 4. The relative difference is smaller than 20% for $\beta = 0.1$. A small peak on the red line is caused by small value of the denominator in the relative difference, see Fig. 3(a).

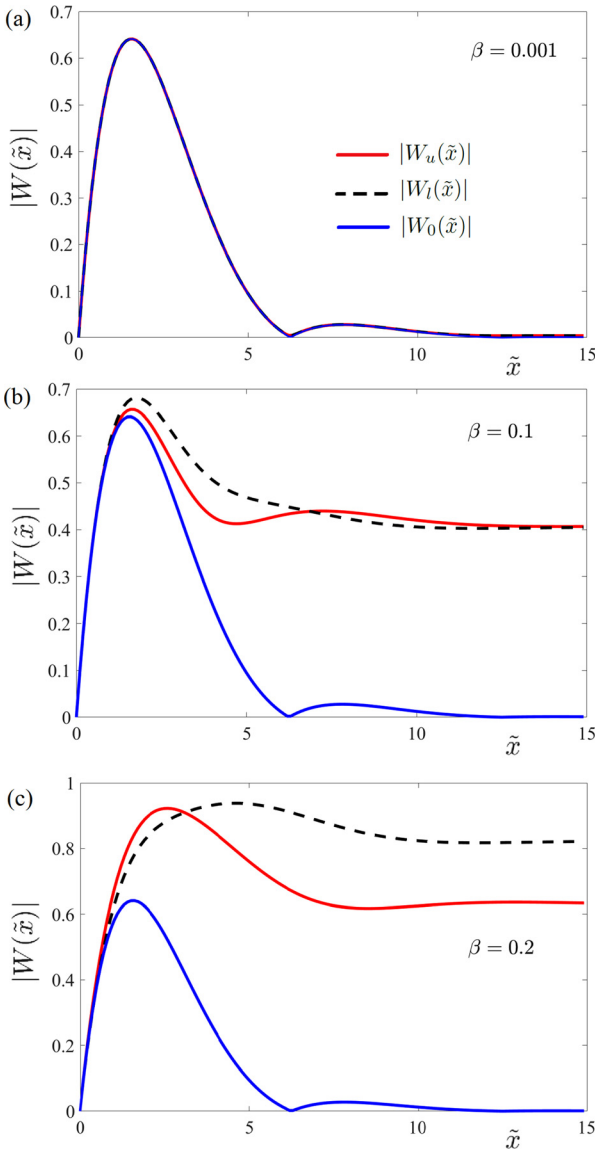

FIG. 3. The deflection amplitudes of the floating poroelastic plate with an oscillating vertical rigid plate without submerged part, $|W_u(\tilde{x})|$ [red lines, Eq. (45)] and by the low-frequency approximation $|W_l(\tilde{x})|$ with two terms [dashed lines, Eq. (26)] and with the leading approximation $|W_0(\tilde{x})|$ only [blue lines, Eq. (28)] for dimensionless frequencies (a) $\beta = 0.001$, (b) $\beta = 0.1$, and (c) $\beta = 0.2$.

To investigate the effect of frequency β on the floating plate deflection, the deflection amplitudes of the floating poroelastic plate $|W_u(\tilde{x})|$, dry plate $|W_d(\tilde{x})|$, and zero porosity plate $W_v(\tilde{x})$ are shown in Fig. 5 for four different frequencies with $\alpha = 10^{-4}$ m^2 s/kg. It is seen that the maximum deflection of poroelastic plate is always higher than the maximum deflection of the corresponding plate without porosity and the maximum occurs close to the excitation place. Far from this place, the deflection of the plate with zero porosity is higher that the deflection of the poroelastic plate for large frequency, see Figs. 5(b)–5(d), and smaller for low frequencies, see Fig. 5(a). The deflections of floating plates are

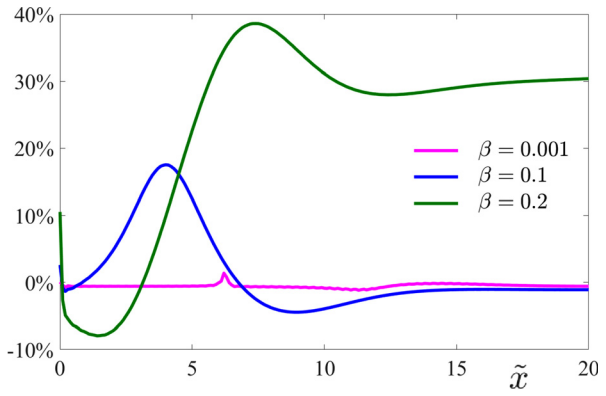

FIG. 4. The relative difference, $100\%(|W_u(\tilde{x})| - |W_l(\tilde{x})|)/|W_u(\tilde{x})|$, between the complete deflection $|W_u(\tilde{x})|$ and the two-term low-frequency approximation (26) for dimensionless frequency $\beta = 0.001$ (magenta line), $\beta = 0.1$ (blue line), and $\beta = 0.2$ (green line).

always smaller that deflection of the dry plate for the same excitation conditions. The parameter γ responsible for the porosity of the plate can be written as $\gamma = (\alpha/\beta)\rho\sqrt{gH}$. For conditions of Fig. 5, the product $\alpha\rho\sqrt{gH} \approx 1$ and, therefore, $\gamma \approx 1/\beta$. We may expect that the effect of the plate porosity becomes stronger for larger γ and weaker for small γ. If we increase the frequency β further, then γ decreases and red lines for poroelastic plate will approach the blue dashed lines for floating plate with zero porosity. Therefore, the attenuation, which is the rate of the deflection decay with the distance $\tilde{x}$, decreases with increase in the frequency and/or decrease in the porosity. However, if we decrease the frequency β or increase the porosity coefficient γ, we should not expect that the porosity becomes stronger. The condition (18) can be written in the form

$$\frac{\partial \Phi}{\partial \tilde{y}} = W(\tilde{x}) + i\gamma P(\tilde{x}), \tag{72}$$

where $P(\tilde{x})$ is the hydrodynamic pressure action on the plate/liquid interface. This condition for large γ gives $P(\tilde{x}) \approx 0$, and then the plate equation (15) becomes the equation of the dry plate. For small γ, Eq. (72) shows that the term with the pressure can be neglected in the leading order, which implies that the poroelastic deflections $|W_u(\tilde{x})|$ should converge to elastic deflections $|W_v(\tilde{x})|$ as $\gamma \to 0$. This situation is illustrated in Fig. 6, where $\beta = 1$ and the deflection amplitudes calculated for different values of γ are shown. It is seen that the poroelastic deflections $|W_u(\tilde{x})|$ converges to the deflection of the elastic floating plate $|W_v(\tilde{x})|$ for small γ and to the deflection of the elastic dry plate $|W_d(\tilde{x})|$ for large γ. It is seen that large porosity does not mean large damping of the generated waves. The deflections in the far field are larger for floating plates with large porosity.

To show that the decay rate of the generated waves is not monotonic with respect to the porosity parameter γ, the deflection amplitude $|W_u(\tilde{x})|$ at $\tilde{x} = 30$, which is far enough from the excitation place, see Fig. 6, is plotted as a function of the porosity parameter $\log_{10}\gamma$ in Fig. 7 in the logarithmic scale. The dimensionless frequency is $\beta = 0.5$. It is seen that the porosity reduces the deflection amplitude in

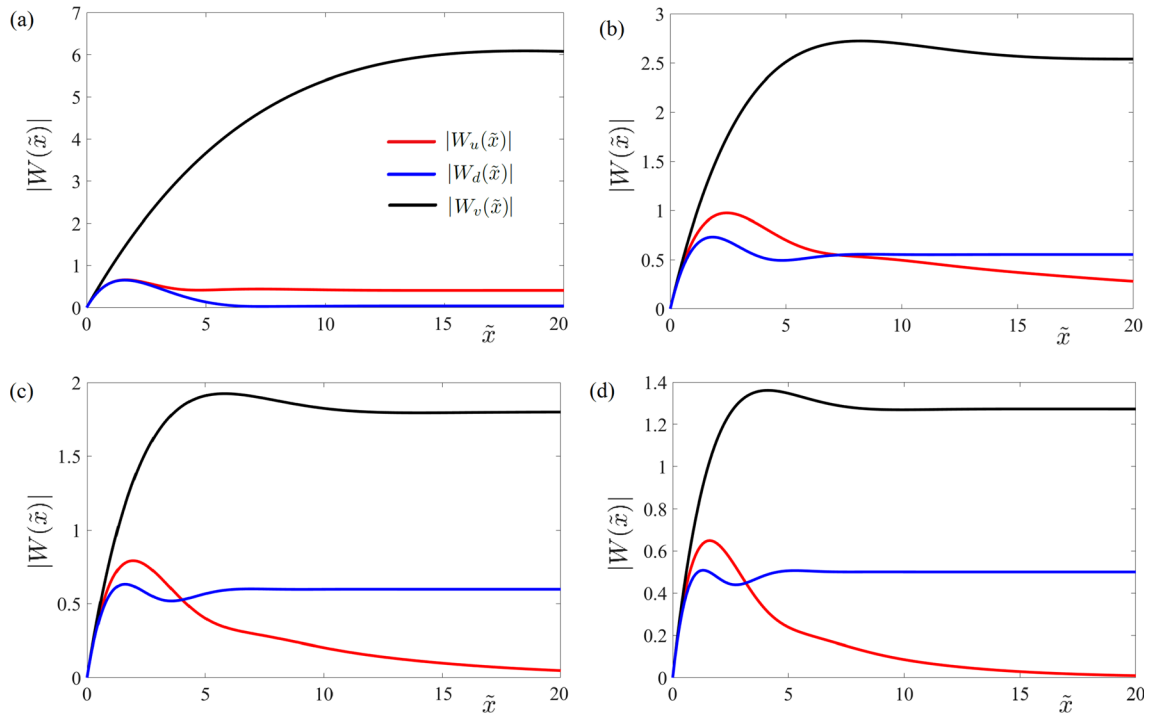

FIG. 5. The amplitudes of the floating poroelastic plate with an oscillating vertical rigid plate without submerged part for poroelastic plate [red lines, Eq. (45)], for dry plate [black lines, Eq. (24)], and for the plate with zero porosity [blue lines, Eq. (54)], for dimensionless frequencies (a) $\beta = 0.1$, (b) $\beta = 0.5$, (c) $\beta = 1$, and (d) $\beta = 2$.

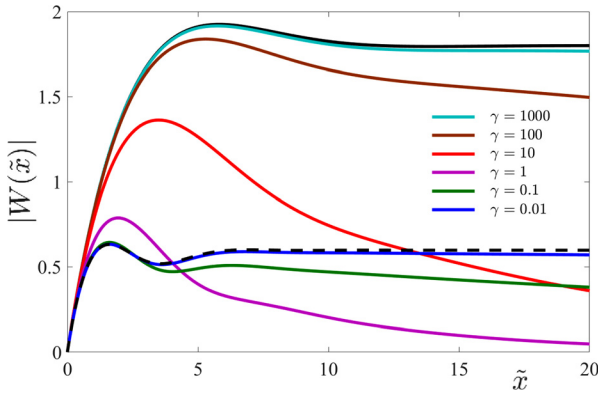

FIG. 6. The deflection amplitudes of floating poroelastic plate, $|W_u(\tilde{x})|$, for different values of the porosity parameter γ and $\beta = 1$, are compared with the deflection of the dry plate $|W_d(\tilde{x})|$ (black solid lines) and with deflection of the plate with zero porosity $|W_v(\tilde{x})|$ (black dashed lines).

the far field only in the interval $0.01 < \gamma < 10$ compared with the elastic plate deflection. If the porosity is greater than 10^4, then the poroelastic plate behaves as a dry plate, see also Fig. 7.

We find that the attenuation of poroelastic plate can be neglected for $\gamma < 2 \times 10^{-2}$, which is for $\alpha < 10^{-5}$ m^2 s/kg, where the behavior of poroelastic plate is close to that of the elastic plate. Similarly, the poroelastic plate can be approximately treated as a dry plate for $\gamma > 200$, which is for $\alpha > 10^{-1}$ m^2 s/kg, where the attenuation does not exist.

The maximum values of the deflection amplitudes, $\max|W(\tilde{x})|$, where $\tilde{x} \geq 0$, and the places where they are achieved, $\tilde{x}_{\max}$, depend on the frequency and porosity for constant other parameters of the problem. These values and positions are important to estimate the maximum energies of the plate and the places where damage is most likely to occur, respectively. The maximum deflection amplitudes $\max|W(\tilde{x})|$ and the positions where they are achieved are shown in Fig. 8 for the dimensionless frequency is $\beta = 0.5$ as functions of the porosity parameter γ. It is seen that the maximum deflection of the

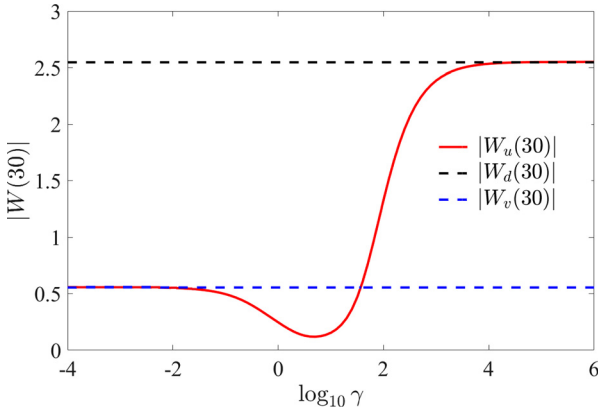

FIG. 7. The deflection amplitude $|W_u(30)|$ (red line) of the floating poroelastic plate at $\tilde{x} = 30$ as a function of the porosity parameter $\log_{10}\gamma$ in the logarithmic scale. The deflection amplitudes at the same point for dry plate (dashed black line) and for the plate with zero porosity (blue dashed line) are shown for reference.

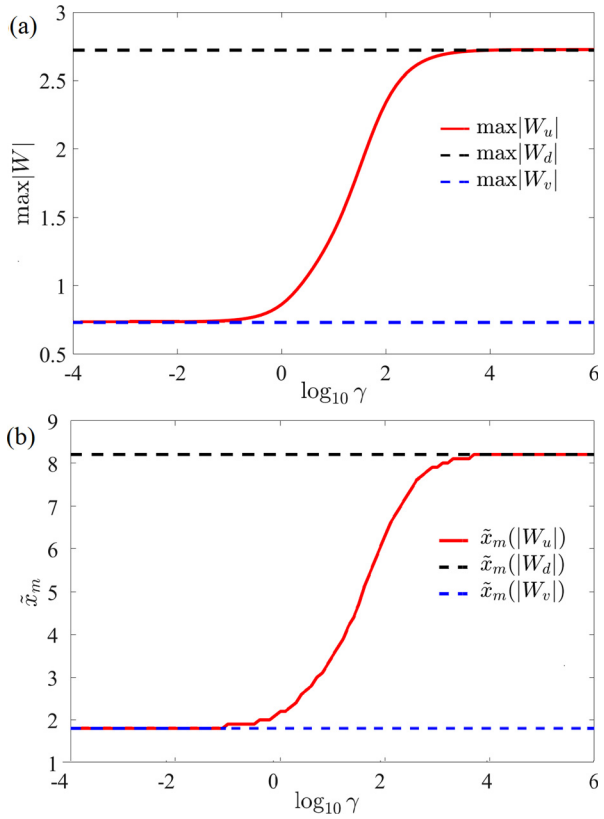

FIG. 8. The maximum deflection amplitude (a) and the position (b), where the maximum deflection is achieved as functions of the porosity parameter γ. Red lines are for poroelastic plate, blue dashed lines for the elastic plate, and black dashed lines are for the dry plate.

poroelastic plate is close to the maximum deflection of the corresponding elastic floating plate and achieved at the same place for $\gamma < 0.02$ and close to the maximum deflection of the dry plate for $\gamma > 200$. The maximum deflection of a poroelastic plate increases and occurs further from the excitation place as porosity increases. This implies that the presence of water under the plate restricts propagation of the energy from the excitation place.

The results for the oscillating vertical rigid plate with long submerged part are shown in Figs. 9–12. The solutions from Sec. IV are used. For small γ, Eq. (72) for rigid plates with and without their submerged parts indicates that the term with the pressure can be neglected in the leading order, which implies that the poroelastic deflections $|W_s(\tilde{x})|$ should converge to elastic deflections $|W_z(\tilde{x})|$ as $\gamma \to 0$. This is shown in Fig. 9, where $\beta = 1$ and the deflection amplitudes calculated for different values of γ are shown. It is seen that the poroelastic deflections $|W_s(\tilde{x})|$ converge to the deflection of the elastic floating plate $|W_z(\tilde{x})|$ for small γ and to the deflection of the elastic dry plate $|W_d(\tilde{x})|$ for large γ. Therefore, large porosity does not mean large damping of the generated waves. The deflections in the far field are larger for floating plates with large porosity.

Figure 9 is similar to Fig. 6, where the poroelastic plate deflections $|W_s(\tilde{x})|$ are shown for the rigid oscillating plate without submerged

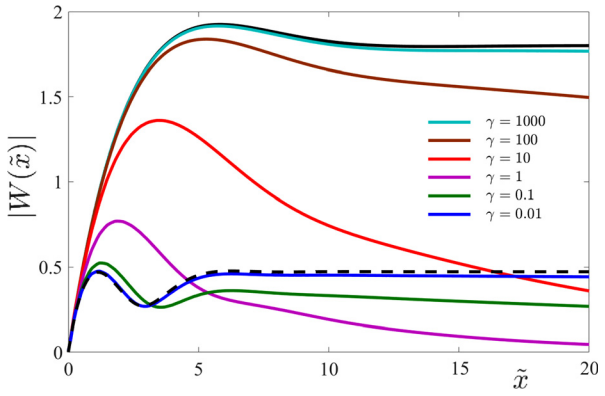

FIG. 9. The deflection amplitudes of the floating poroelastic plate, $|W_s(\tilde{x})|$, shown by color lines for different values of the porosity parameter γ, are compared with the deflection of the dry plate $|W_d(\tilde{x})|$ (black solid line) and with deflection of the plate with zero porosity $|W_z(\tilde{x})|$ (black dashed line), for the rigid plate with long submerged part and $\beta = 1$.

part. The deflection amplitudes of floating poroelastic plate, $|W_u(\tilde{x})|$, without submerged part of the oscillating plate and the deflection amplitudes, $|W_s(\tilde{x})|$, for the rigid oscillating plate with long submerged part are compared for different values of the porosity parameter γ for $\beta = 0.5$ in Fig. 10. It is seen that the effect of the submerged part of the rigid plate is negligible for large porosity, $\gamma > 1$. For small porosity, the presence of the rigid plate in water reduces the floating poroelastic plate deflections.

The decay rate of the generated waves for the oscillating rigid plate with long submerged part is not monotonic with respect to the porosity parameter γ, see Fig. 11. In this figure, the amplitude $|W_s(\tilde{x})|$, at $\tilde{x} = 30$ is plotted as a function of the porosity parameter $\log_{10}\gamma$ in the logarithmic scale. It is seen that the porosity reduces the deflection amplitude in the far field only in the interval $0.01 < \gamma < 10$ compared with the elastic plate deflection. This figure is similar to Fig. 7, which is for the deflection amplitude $|W_u(30)|$ without submerged part of the oscillating rigid plate.

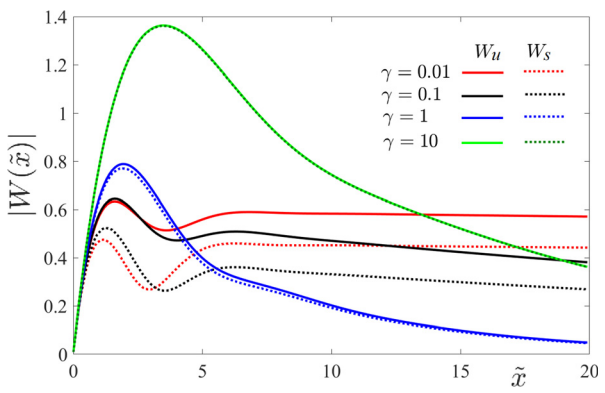

FIG. 10. The deflection amplitudes of floating poroelastic plate, $|W_u(\tilde{x})|$, without submerged part of the oscillating plate (solid lines) and the deflection amplitudes, $|W_s(\tilde{x})|$, for the rigid oscillating plate with long submerged part (dashed lines) are compared for different values of the porosity parameter γ for $\beta = 0.5$.

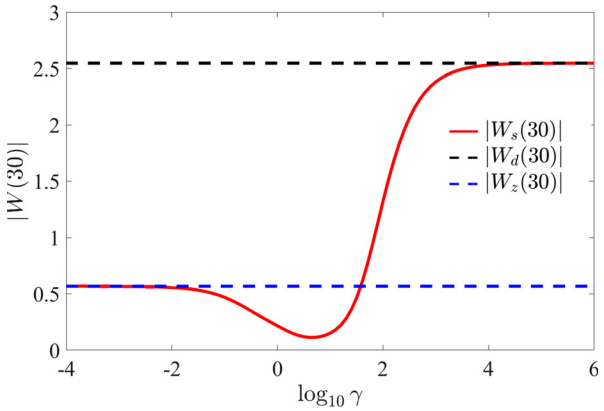

FIG. 11. The deflection amplitude $|W_s(30)|$ (red line) of the floating poroelastic plate at $\tilde{x} = 30$ as a function of the porosity parameter $\log_{10}\gamma$ in the logarithmic scale. The deflection amplitudes at the same point for dry plate (dashed black line) and for the plate with zero porosity (blue dashed line) are shown for reference.

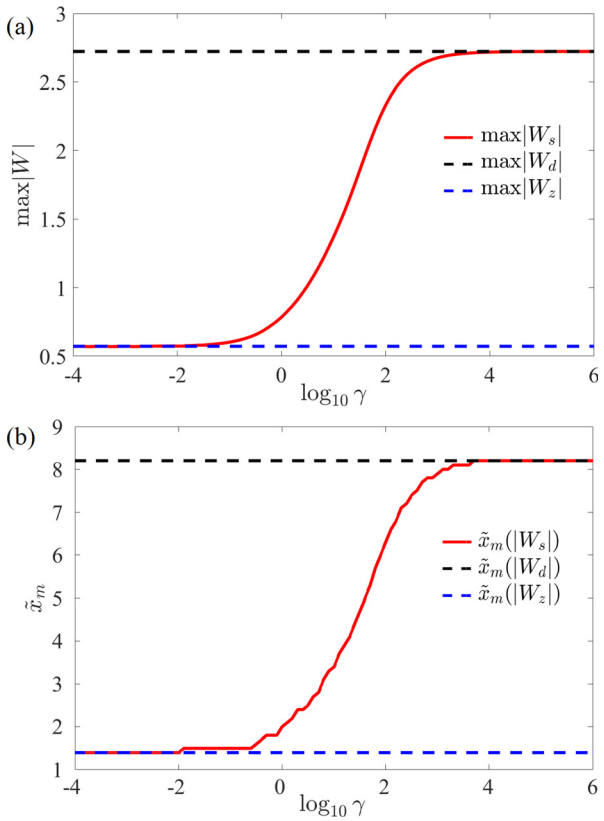

FIG. 12. The maximum deflection amplitude (a) and the position (b), where the maximum deflection is achieved, as a function of the porosity parameter γ for the oscillating rigid plate with a long submerged part. Red lines are for the poroelastic plate, blue dashed lines for the elastic plate, and black dashed lines are for the dry plate.

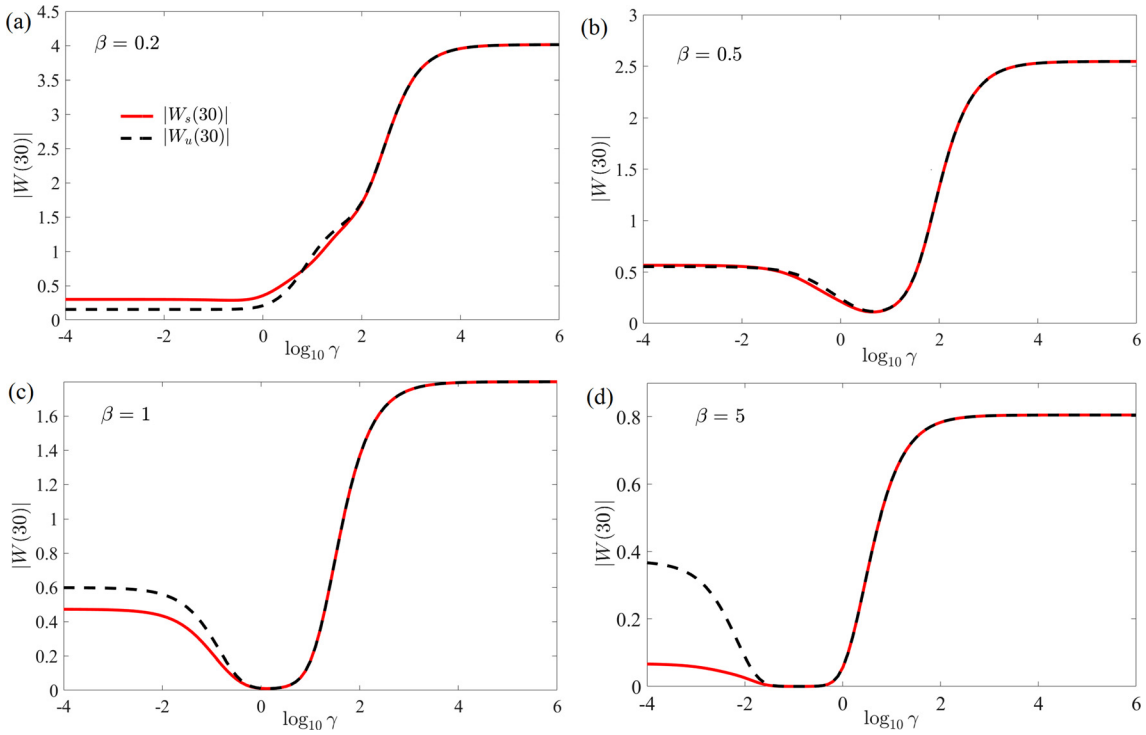

FIG. 13. The deflection amplitudes with (red lines) and without (black dashed lines) submerged part of the oscillating rigid plate at $\tilde{x} = 30$ as functions of the porosity parameter γ for dimensionless frequencies (a) $\beta = 0.2$, (b) $\beta = 0.5$, (c) $\beta = 1$, and (d) $\beta = 5$.

The maximum values of the deflection amplitudes, $\max|W_s(\tilde{x})|$, where $\tilde{x} \geq 0$, and the places where they are achieved, $\tilde{x}_{\max}$, depend on the frequency and porosity for constant other parameters of the problem. The maximum deflection amplitudes $\max|W_s(\tilde{x})|$ and the positions where they are achieved are shown in Fig. 12 for dimensionless frequency is $\beta = 0.5$ as functions of the porosity parameter γ. It is seen that the maximum deflection of the poroelastic plate is close to the maximum deflection of the corresponding elastic floating plate and achieved at the same place for $\gamma < 0.02$ and close to the maximum deflection of the dry plate for $\gamma > 200$. The maximum deflection of a poroelastic plate increases and occurs further from the excitation place as the porosity increases. This implies that the presence of water under the plate restricts propagation of the energy from the excitation place. This figure is similar to Fig. 8, which is for the deflection amplitude $|W_u(30)|$ without submerged part of the oscillating rigid plate.

The effect of the frequency is strong which is clear from Figs. 3–5. The deflection amplitudes with, $|W_s(30)|$, and without, $|W_u(30)|$, submerged part of the oscillating rigid plate at $\tilde{x} = 30$ are shown as functions of the porosity parameter γ for different dimensionless frequencies β in Fig. 13. Both deflection amplitudes are monotonic functions of γ for small frequencies, see Fig. 13(a). Note that $|W_s(30)| < |W_u(30)|$ for $\beta = 0.2$ and $\gamma < 1$. For larger frequency $|W_s(30)| \approx |W_u(30)|$ for all values of γ for $\beta = 0.5$, for $\gamma > 1$ for $\beta = 1$, and for $\gamma > 0.1$ for $\beta = 5$. There are intervals of the porosity parameter for large frequencies, where $|W_s(30)| \approx |W_u(30)| \approx 0$, see Figs. 13(c) and 13(d). For large frequencies and small porosity, the deflections in the far field are greater for the oscillating rigid plate with the long submerged part.

The distributions of the scaled strain amplitudes in the floating poroelastic plate with, $|\varepsilon_s(\tilde{x})|/\varepsilon_{sc}$, and without, $|\varepsilon_u(\tilde{x})|/\varepsilon_{sc}$, submerged part of the oscillating rigid plate are shown in Fig. 14 for $\beta = 0.5$ and $\gamma = 2$. The scale is given in (20). It is seen that the maximum strain is achieved at the place of the excitation, where the $|\varepsilon_s(0)| > |\varepsilon_u(0)|$.

The amplitudes of the deflections and strains predicted by Meylan's and Zavyalova's models are compared in Fig. 15 for different frequencies and the pitching rigid plate without its submerged part. The deflections and strains are calculated by using Eqs. (45) and (46) correspondingly with $\delta = 0$ for Meylan's model and $\delta = 1$ for

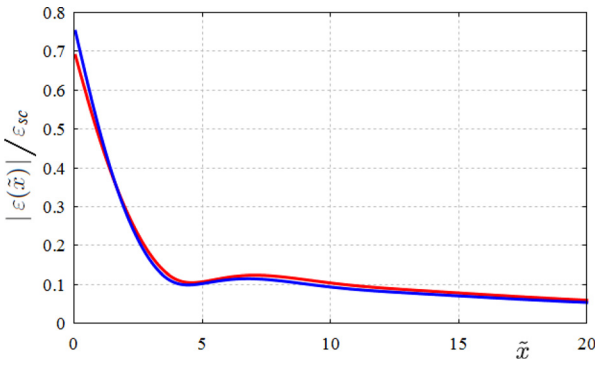

FIG. 14. The amplitudes of scaled strains in the floating poroelastic plate calculated for the pitching vertical plate long submerged part, $|\varepsilon_s(x)|/\varepsilon_{sc}$, (blue line) and without the vertical plate in liquid, $|\varepsilon_u(x)|/\varepsilon_{sc}$, (red line) for $\beta = 0.5$ and $\gamma = 2$.

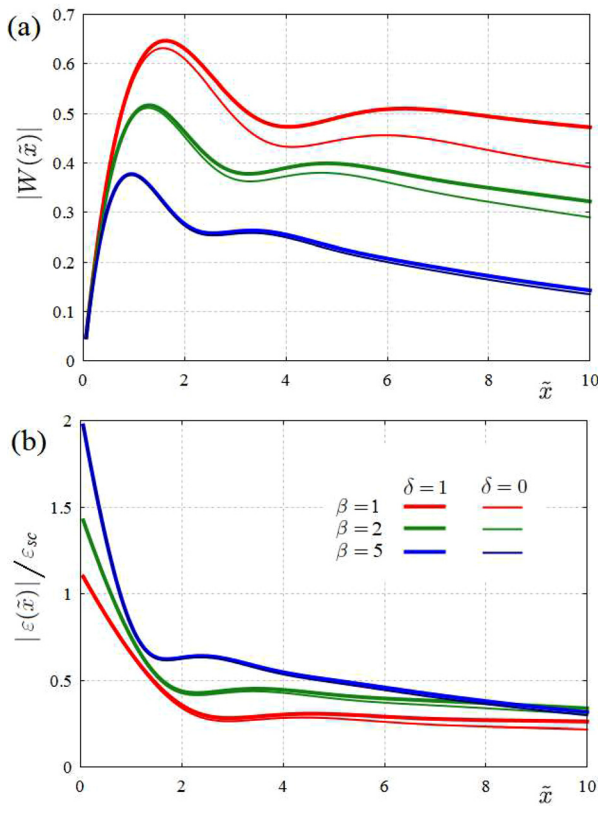

FIG. 15. The dimensionless deflection, $|W_u(x)|$, (a) and scaled strain, $|\varepsilon_u(x)|/\varepsilon_{sc}$, (b) amplitudes of floating poroelastic plate calculated within Zavyalova's (thick lines) and Meylan's (thin lines) models for $\alpha = 10^{-5}$ m^2 s/kg and different frequencies β given in the inlet (b).

Zavyalova's model in (41). The results by these models are close one to another for large frequencies, and this is for large γ, see Eq. (42), and deviate one from another for smaller frequencies. The differences between predictions by the two models increase with a decrease in the dimensionless frequency β and an increase in the porosity parameter α.

The ice is assumed to break there where the amplitude of the strain $|\varepsilon(\tilde{x})|$ approaches the so-called yield strain of ice, which is estimated as 8×10^{-5}, see Brocklehurst *et al.* (2011). In the conditions of the present calculations with ice thickness 1 m and water depth 10 m, we have $\varepsilon_{sc} = \theta/20$, see Eq. (20). The yield strain is achieved for $\beta = 1$ at the amplitude of the rigid plate oscillations $\theta = 0.076°$, and for $\beta = 5$ at the amplitude $\theta = 0.0046°$ at the place, where the rigid plate is built in the floating plate, see Fig. 15. Note that the angle of the plate inclination θ is in radians in Eq. (20). The derived estimates of the maximum values of the angle of the rigid plate inclination before breaking the floating ice plate justify the linear approximation employed in this study because the allowed angles and the resulting deflections are very small [Cho and Kim (2008); Chwang and Li (1983); Cox and Weeks (1983); Ward *et al.* (2017); Korobkin *et al.* (2018); Manam and Sivanesan (2016); (2017); and Taylor (1956)].

VI. CONCLUSION

Two-dimensional periodic deflection of a floating poroelastic plate has been investigated within Meylan's and Zavyalova's models of floating poroelastic plates. The floating plate was governed by the equation of thin elastic plate. Porosity was accounted through the influx of the liquid into the floating plate. The velocity of the influx was taken to be proportional to the hydrodynamic pressure on the plate/liquid interface. This pressure in the porosity model is the complete pressure which is the same as acting on the floating plate within the Zavyalova's model and only the dynamic pressure component within Meylan's model. As the authors are unaware of experimental results with poor realistic floating plates, where a porosity model is justified. Correspondingly, we do not know which model of floating paralytic plate is the best one. Our investigation of these two simplest models discovered several predictions which are different within different models. Such theoretical results may help to design future experiments with poroelastic plates and select conditions of experiments leading to the most reliable model. Note that in the present formulation, the upper surface of the floating plate is always dry, and the lower surface of the plate is always in contact with the liquid. This is possible only if the amplitude of the plate deflection is much smaller than the plate thickness. It was shown that both models provide identical results for large frequencies and small porosities. Further investigations are needed, including experimental ones, to arrive at a physically reliable models of floating poroelastic plates.

The flexural gravity waves in the floating plate were generated by a rigid thin plate built in the floating plate and swinging at a given frequency with a given small amplitude. This problem is coupled with the plate deflection and hydrodynamic loads to be determined at the same time. Two cases were distinguished with the rigid swinging plate being strictly above the liquid (case 1) and under the floating plate extended to the liquid bottom (case 2). The problem for the first case was formulated in Sec. II and solved within different approximations in Secs. III and IV, the formulation was extended to the swinging plate with the long submerged part, and the problem for the second case was solved within Fourier transform for non-zero porosity and using the vertical modes for elastic plate with zero porosity. In both cases, the problems were solved for elastic plates with non-zero and zero porosities.

The behavior of the floating poroelastic plate for a given excitation was studied in Sec. V within different models and approximations. It was shown that the rate of decay of the plate deflection with the distance from the excitation place is not a monotonic function of the porosity parameter. This result, in terms of the wave energy dissipation, was reported by Meylan *et al.* (2017). In the present study, we found that the plate behaves as an elastic one with zero porosity for small values of the porosity parameter. Correspondingly, the decay rate of the generated wave is small. For large porosity with large opening of the pores, the pressure under the plate is close to the atmospheric pressure and the plate deflection is weakly depend on the presence of the liquid. The numerical results confirm this finding.

Energy balance relations were not analyzed in this study. The energy dissipates because of the plate porosity. It would be interesting to obtain proportions between the bending energy of the plate, kinetic energy of the plate, kinetic energy of the flow under the plate, and the potential energy of the flow for different excitation conditions and different models.

ACKNOWLEDGMENTS

This work was supported by the National Natural Science Foundation of China (Grant Nos. 52192693, 52192690, 51979051, 51979056, and U20A20327) and the National Key Research and Development Program of China (No. 2021YFC2803400), to which the authors are most grateful.

AUTHOR DECLARATIONS

Conflict of Interest

The authors have no conflicts to disclose.

Author Contributions

Qiyuan Wu: Conceptualization (equal); Data curation (equal); Formal analysis (equal); Investigation (equal); Software (equal); Validation (equal); Visualization (equal); Writing – original draft (equal); Writing – review & editing (equal). **Tatyana Khabakhpasheva:** Conceptualization (equal); Data curation (equal); Formal analysis (equal); Investigation (equal); Methodology (equal); Validation (equal); Visualization (equal); Writing – original draft (equal); Writing – review & editing (equal). **Baoyu Ni:** Conceptualization (equal); Funding acquisition (equal); Investigation (equal); Methodology (equal); Project administration (equal); Resources (equal). **Alexander Korobkin:** Conceptualization (equal); Formal analysis (equal); Investigation (equal); Methodology (equal); Supervision (equal); Validation (equal); Writing – original draft (equal); Writing – review & editing (equal).

DATA AVAILABILITY

The data that support the findings of this study are available within the article.

REFERENCES

Ashok, R., Gunasundari, C., and Manam, S. R., "Explicit solutions of the scattering problems involving vertical flexible porous structures," J. Fluids Struct. **99**, 103149 (2020).
Biot, M., "Theory of propagation of elastic waves in a fluid saturated porous solid. I Low frequency range," J. Acoust. Soc. Am. **28**, 168–178 (1956a).
Biot, M., "Theory of propagation of elastic waves in a fluid saturated porous solid. II. Higher frequency range," J. Acoust. Soc. Am. **28**, 179–191 (1956b).
Brocklehurst, P., Korobkin, A. A., and Parau, E. I., "Interaction of hydro-elastic waves with a vertical wall," J. Eng. Math. **68**(3–4), 215–231 (2010).
Brocklehurst, P., Korobkin, A. A., and Parau, E. I., "Hydroelastic wave diffraction by a vertical cylinder," Philos. Trans. R. Soc., A **369**(1947), 2832–2851 (2011).
Chanda, A. and Bora, S. N., "Investigation of oblique flexural gravity wave scattering by two submerged thin vertical porous barriers with different porosities," J. Eng. Mech. **148**(2), 04021145 (2021a).
Chanda, A. and Bora, S. N., "Scattering of flexural gravity waves by a pair of submerged vertical porous barriers located above a porous sea-bed," J. Offshore Mech. Arct. Eng. **144**(1), 011201 (2021b).
Chen, H., Gilbert, R. P., and Guyenne, P., "Dispersion and attenuation in a porous viscoelastic model for gravity waves on an ice-covered ocean," Eur. J. Mech.-B/Fluids **78**, 88–105 (2019).
Cho, I. H. and Kim, M. H., "Wave absorbing system using inclined perforated plates," J. Fluid Mech. **608**, 1–2 (2008).
Cho, I. H. and Kim, M. H., "Transmission of oblique incident waves by a submerged horizontal porous plate," Ocean Eng. **61**, 56–65 (2013).
Cho, I. H., Koh, H. J., Kim, J. R., and Kim, M. H., "Wave scattering by dual submerged horizontal porous plates," Ocean Eng. **73**, 149–158 (2013).
Chwang, A. T. and Chan, A. T., "Interaction between porous media and wave motion," Annu. Rev. Fluid Mech. **30**(1), 53–84 (1998).
Chwang, A. T. and Li, W., "A piston-type porous-wavemaker theory," J. Eng. Math. **17**, 301–313 (1983).
Chwang, A. T. and Wu, J., "Wave scattering by submerged porous disk," J. Eng. Mech. **120**(12), 2575–2587 (1994).
Cox, G. F. and Weeks, W. F., "Equations for determining the gas and brine volumes in sea-ice samples," J. Glaciol. **29**(102), 306–316 (1983).
Dagan, G., *Flow and Transport in Porous Formations* (Springer-Verlag, Berlin, 1989).
Dalrymple, R. A., Losada, M. A., and Martin, P. A., "Reflection and transmission from porous structures under oblique wave attack," J. Fluid Mech. **224**(1), 625 (1991).
Darcy, H. P. G., *Les Fontaines Publiques de la Ville de Dijon* (Dalmont, Paris, 1856).
Eicken, H., Grenfell, T. C., Perovich, D. K., Richter-Menge, J. A., and Frey, K., "Hydraulic controls of summer Arctic pack ice albedo," J. Geophys. Res.: Oceans **109**(C8), C08007, https://doi.org/10.1029/2003JC001989 (2004).
Evans, D. V. and Peter, M. A., "Asymptotic reflection of linear water waves by submerged horizontal porous plates," J. Eng. Math. **69**, 135–154 (2011).
Forchheimer, P., "Wasserbewegung durch boden," Z. Ver. Dtsch. Ing. 49, 1736 (1901).
Freitag, J., "The hydraulic properties of arctic sea-ice: Implications for the small scale particle transport," Rep. Polar Res. **325**, 170 (1999).
Gayen, R. and Mondal, A., "A hypersingular integral equation approach to the porous plate problem," Appl. Ocean Res. **46**, 70–78 (2014).
Gradshteyn, I. S. and Ryzhik, I. M., *Table of Integrals, Series, and Products* (Academic Press, 2014).
Haber, S. and Mauri, R., "Boundary conditions for Darcy's flow through porous medium," Int. J. Multiphase Flow **9**(5), 561–574 (1983).
Koley, S., Kaligatla, R. B., and Sahoo, T., "Oblique wave scattering by a vertical flexible porous plate," Stud. Appl. Math. **135**(1), 1–34 (2015).
Koley, S., Mondal, R., and Sahoo, T., "Fredholm integral equation technique for hydroelastic analysis of a floating flexible porous plate," Eur. J. Mech.-B/Fluids **67**, 291–305 (2018).
Korobkin, A. A., Malenica, S., and Khabakhpasheva, T. I., "Interaction of flexural-gravity waves in ice cover with vertical walls," Philos. Trans. R. Soc., A **376**(2129), 20170347 (2018).
Korobkin, A. A., Malenica, S., and Khabakhpasheva, T. I., "The vertical mode method in the problems of flexural-gravity waves diffracted by a vertical cylinder," Appl. Ocean Res. **84**, 111–121 (2019).
Kumar, P. S. and Sahoo, T., "Wave interaction with a flexible porous breakwater in a two-layer fluid," J. Eng. Mech. **132**(9), 1007–1014 (2006).
Liu, Y., Li, H. J., and Li, Y. C., "A new analytical solution for wave scattering by a submerged horizontal porous plate with finite thickness," Ocean Eng. **42**, 83–92 (2012).
Liu, Y. and Li, Y. C., "An alternative analytical solution for water-wave motion over a submerged horizontal porous plate," J. Eng. Math. **69**(4), 385–400 (2011).
Liu, Y., Li, Y. C., Teng, B., and Dong, S., "Wave motion over a submerged breakwater with an upper horizontal porous plate and a lower horizontal solid plate," Ocean Eng. **35**(16), 1588–1596 (2008).
Luong, V. H. and Nguyen, H. P., "Application of quadratic pressure drop condition in hydroelastic analysis of floating structures protected by perforated barrier," Eng. Anal. Boundary Elem. **157**, 59–70 (2023).
Manam, S. R., Bhattacharjee, J., and Sahoo, T., "Expansion formulae in wave structure interaction problems," Proc. R. Soc. A **462**(2065), 263–287 (2006).
Manam, S. R. and Sivanesan, M., "Scattering of water waves by vertical porous barriers: An analytical approach," Wave Motion **67**, 89–101 (2016).
Manam, S. R. and Sivanesan, M., "A note on the explicit solutions for wave scattering by vertical porous barriers," Wave Motion **69**, 81–90 (2017).
McIver, P., "The dispersion relation and eigenfunction expansions for water waves in a porous structure," J. Eng. Math. **34**(3), 319–334 (1998).
Meylan, M. H., Bennetts, L. G., and Peter, M. A., "Water-wave scattering and energy dissipation by a floating porous elastic plate in three dimensions," Wave Motion **70**, 240–250 (2017).

Mohapatra, S. C., Sahoo, T., and Soares, G. C., "Surface gravity wave interaction with a submerged horizontal flexible porous plate," Appl. Ocean Res. **78**, 61–74 (2018).
Negi, P., Kar, P., Sahoo, T., and Meylan, M. H., "Flexural gravity wave interaction with an articulated heterogeneous plate within the paradigm of blocking dynamics," Phys. Fluids **35**(8), 086602 (2023).
Ni, B. Y., Khabakhpasheva, T. I., and Semenov, Y. A., "Nonlinear gravity waves in the channel covered by broken ice," Phys. Fluids **35**(10), 102118 (2023).
Panduranga, K., Koley, S., and Meylan, M. H., "A hybrid boundary element method based model for wave interaction with submerged viscoelastic plates with an arbitrary bottom profile in frequency and time domain," Phys. Fluids **35**(4), 047114 (2023).
Patari, S., Chowdhury, I. U., Kumar, J., and Mahapatra, P. S., "Dynamics of liquid flow through fabric porous media: Experimental, analytical, and numerical investigation," Phys. Fluids **35**(10), 103305 (2023).
Petrich, C., Langhorne, P. J., and Sun, Z. F., "Modelling the interrelationships between permeability, effective porosity and total porosity in sea ice," Cold Reg. Sci. Technol. **44**(2), 131–144 (2006).
Philip, J. R., "Flow in porous media," Annu. Rev. Fluid Mech. **2**, 177–203 (1970).
Saffman, P. G., "On the boundary condition at the surface of a porous medium," Stud. Appl. Math. **50**, 93–101 (1971).
Sahoo, T., Yip, T. L., and Chwang, A. T., "Scattering of surface waves by a semi-infinite floating elastic plate," Phys. Fluids **13**(11), 3215–3222 (2001).
Scheidegger, A. E., "Hydrodynamics in porous media," in *Handbuch Der Physik 8/2: Stromungsmechanik*, edited by S. Fugge (Springer-Verlag, Berlin, 1963), pp. 625–662.
Singh, M., Meylan, M. H., and Gayen, R., "Time-domain motion of a floating or obliquely submerged non-uniform elastic plate," Phys. Fluids **35**(4), 047117 (2023).
Smith, M. J. A., Peter, M. A., Abrahams, I. D., and Meylan, M. H., "On the Wiener–Hopf solution of water-wave interaction with a submerged elastic or poroelastic plate," Proc. R. Soc. A. **476**, 20200360 (2020).
Sollitt, C. K. and Cross, R. H., "Wave transmission through permeable breakwaters," Coastal Eng. **1**, 99 (1972).
Squire, V. A., Hosking, R. J., Kerr, A. D., and Langhorne, P. J., *Moving Loads on Ice Plates* (Kluwer Academic Publishers, 1996).
Taylor, G. I., "Fluid flow in regions bounded by porous surfaces," Proc. R. Soc. London, Ser. A **234**(1199), 456–475 (1956).
Wang, K. and Ren, X., "Water waves on flexible and porous breakwaters," J. Eng. Mech. **119**(5), 1025–1047 (1993).
Wang, K. H. and Ren, X., "An effective wave trapping system," Ocean Eng. **21**(2), 155–178 (1994).
Wang, P., Lu, D. Q., and Fu, L. D., "Steady-state hydroelastic waves generated by a moving load in a uniform current," Wave Motion **122**, 103190 (2023).
Ward, J. C., "Turbulent flow in porous media," J. Hydraul. Div. **90**(5), 1–12 (1964).
Ward, N. D. F., Lahivaara, T., and Eveson, S., "A discontinuous Galerkin method for poroelastic wave propagation: The two-dimensional case," J. Comput. Phys. **350**, 690–727 (2017).
Williams, A. N. and Wang, K. H., "Flexible porous wave barrier for enhanced wetlands habitat restoration," J. Eng. Mech. **129**(1), 1–8 (2003).
Wu, J. H., Wan, Z. P., and Fang, Y., "Wave reflection by a vertical wall with a horizontal submerged porous plate," Ocean Eng. **25**(9), 767–779 (1998).
Wu, Q., Khabakhpasheva, T., Ni, B., and Korobkin, A., "Interaction of a flexural-gravity wave with a vertical rigid plate built in a floating elastic plate," J. Mar. Sci. Eng. **11**(4), 697 (2023).
Yip, T. L., Sahoo, T., and Chwang, A. T., "Trapping of surface waves by porous and flexible structures," Wave Motion **35**(1), 41–54 (2002).
Yu, X. and Chwang, A. T., "Water waves above submerged porous plate," J. Eng. Mech. **120**(6), 1270–1282 (1994).
Zavyalova, K. N., Shishmarev, K. A., and Korobkin, A. A., "The response of a poroelastic ice plate to an external pressure," J. Sib. Fed. Univ., Math. Phys. **14**(1), 87–97 (2021).
Zheng, S., Meylan, M., Zhua, G., Greaves, D., and Iglesias, G., "Wave scattering from multiple circular floating porous elastic plates," in Proceedings of *35th International Workshop on Water Waves and Floating Bodies* (IWWWFB 2020), 2020a.
Zheng, S., Meylan, M. H., Zhu, G., Greaves, D., and Iglesias, G., "Hydroelastic interaction between water waves and an array of circular floating porous elastic plates," J. Fluid Mech. **900**, A20 (2020b).
Zheng, S., Meylan, M. H., Fan, L., Greaves, D., and Iglesias, G., "Wave scattering by a floating porous elastic plate of arbitrary shape: A semi-analytical study," J. Fluids Struct. **92**, 102827 (2020c).